Nonlinear Feedback in a Five-Dimensional Lorenz Model

BO-WEN SHEN

Earth System Science Interdisciplinary Center, University of Maryland, College Park, College Park, and NASA Goddard Space Flight Center, Greenbelt, Maryland

(Manuscript received 22 July 2013, in final form 3 December 2013)

ABSTRACT

In this study, based on the number of modes, the original three-dimensional Lorenz model (3DLM) is generalized with two additional modes [five-dimensional Lorenz model (5DLM)] to examine their role in the predictability of the numerical solutions and to understand the underlying processes that increase the solution stability. As a result of the simplicity of the 5DLM with respect to existing generalized Lorenz models (LMs), the author is able to obtain the analytical solutions of its critical points and identify the role of the major nonlinear term in the solution's stability, which have previously not been documented in the literature. The nonlinear Jacobian terms of the governing equations are analyzed to highlight the importance of selecting new modes for extending the nonlinear feedback loop of the 3DLM and thus effectively increasing the degree of nonlinearity (i.e., the nonlinear mode–mode interactions) in the 5DLM. It is then shown that numerical solutions in the 5DLM require a larger normalized Rayleigh number r for the onset of chaos and are more predictable than those in the 3DLM when r is between 25 and 40 and the Prandtl number σ is 10. The improved predictability is attributable to the negative nonlinear feedback enabled by the new modes. The role of the (negative) nonlinear feedback is further verified using a revised 3DLM with a parameterized nonlinear eddy dissipative term. The finding of the increased stability in the 5DLM and revised 3DLM with respect to the 3DLM is confirmed with the linear stability analysis and the analysis of the Lyapunov exponents using different values of r and σ. To further understand the impact of an additional heating term, results from the 5DLM and a higher-dimensional LM [e.g., the six-dimensional LM (6DLM)] are analyzed and compared.

1. Introduction

Since the 1960s, when Lorenz presented the sensitive dependence of numerical solutions on initial conditions (ICs) with simplified governing equations describing a two-dimensional, forced, dissipative Rayleigh–Benard convection, it has been widely recognized that perfect deterministic weather predictions are impossible. In his breakthrough modeling study where three spatial Fourier modes were used to represent the streamfunction and temperature perturbations of the convection, Lorenz (1963a) showed that numerical results become chaotic, with sensitivities to ICs, when a normalized Rayleigh number r exceeds a critical number (e.g., $r_c = 24.74$ for a constant Prandtl number $\sigma = 10$). This model is referred to as a three-dimensional Lorenz model (3DLM) in the present study. Lorenz associated the chaotic behavior with the inclusion of the nonlinearity. Subsequent to his follow-up presentation in 1972 (Lorenz 1972), the term "butterfly effect" was introduced to describe the sensitive dependence on ICs; later this became a metaphor (or symbol) for indicating that small-scale perturbations can make a huge impact on large-scale flows. In this study, the former and latter definitions are referred to as the butterfly effect of the first and second kind, respectively. The studies by Lorenz laid the foundation for chaos theory, which was viewed as the third scientific revolution of the twentieth century after relativity and quantum mechanics and is being applied in various fields including earth science, mathematics, philosophy, and physics (e.g., Gleick 1987; Anthes 2011).

Since the publications of Lorenz (1963a, 1972), views regarding the predictability of weather and climate have been significantly influenced by the butterfly effect (of the first and second kinds) or chaos theory (Solomon et al. 2007, 96–97; Pielke 2008). It is well accepted that weather is chaotic with only a finite predictability, and it

Denotes Open Access content.

Corresponding author address: Dr. Bo-Wen Shen, Mesoscale Atmospheric Processes Laboratory, Code 612, NASA Goddard Space Flight Center, Greenbelt, MD 20771.
E-mail: bo-wen.shen-1@nasa.gov

DOI: 10.1175/JAS-D-13-0223.1

is believed that the source of chaos in the 3DLM is the nonlinearities. Based on this understanding, one might expect that solutions to the equations with more nonlinear modes would become more chaotic, equivalent to stating that the appearance of small-scale features and their nonlinear effects, resolved by the additional modes, may make the system more chaotic. Since high-resolution global modeling approaches (e.g., Atlas et al. 2005; Shen et al. 2006a,b), which require tremendous computing resources, have become a current trend for weather prediction and climate projection, it becomes important to understand the role of the increased resolutions in the solution's stability (or predictability) of the models. Three kinds of predictability that were proposed by Lorenz (1963b) include 1) intrinsic predictability that is dependent only on a flow itself, 2) attainable predictability that is limited by the imperfect initial conditions, and 3) practical predictability that shows dependence on (mathematical) formulas. The last type is discussed in this study by deriving a generalized Lorenz model (LM) and comparing its predictability with that of the 3DLM. In the literature, the term "a generalized LM" has been used to refer to the model that has modes more than the 3DLM.

Previous studies with the inclusion of additional Fourier modes have suggested that a larger r is required for the onset of chaos in generalized LMs [e.g., r_c of approximately 43.5 in the generalized LM with 14 modes (Curry 1978)]. As compared to the aforementioned studies, a more systematic study for examining the resolution dependence of chaotic solutions was conducted numerically by Curry et al. (1984). They observed an irregular change in the degree of chaos as the resolution increased from a low resolution (i.e., three Fourier modes) and obtained a steady-state solution with sufficiently high resolution. However, as the resolution of the numerical weather models is finite and has always been increasing incrementally, it is important to understand the role of the incremental degree of nonlinearity in the solution's stability. The term "degree of nonlinearity" is loosely defined as the degree of mode–mode interactions and is introduced to emphasize that the nonlinearities in numerical models such as the 3DLM are truncated (or finite) as a result of mode truncation. A more specific definition is given in section 3a. In a recent study of the routes to chaos in generalized LMs, Roy and Musielak (2007a) emphasized the importance in selecting modes that can conserve the system's energy in the dissipationless limit. Furthermore, by analyzing the onset of chaos in the 3DLM and different generalized LMs with five and up to nine modes, Roy and Musielak (2007a,b,c) reported that some generalized LMs required a larger r ($r_c \sim 40$) for the onset of chaos, but others displayed a comparable (e.g., $r_c \sim 24.74$ in one of their LMs with six modes) or even a smaller r_c (e.g., $r_c \sim 22$ in their LM with five modes). The aforementioned studies give an inconclusive answer to the question of whether higher-dimensional LMs are more stable (predictable). A possible reason for this discrepancy among existing generalized LMs is presumably related to the various truncations of modes, leading to different degrees of nonlinearity. This is addressed using the following question in this study: under which conditions could the increased degree of nonlinearity improve solution stability? We will address this question with generalized LMs in this study.

In this study, we extend the 3DLM to the five-dimensional LM (5DLM) by including two additional Fourier modes with two additional vertical wavenumbers. In a companion paper (B.–W. Shen 2013, unpublished manuscript), we extend the 5DLM to the six-dimensional LM (6DLM) with an additional mode. Although the nonlinear mode–mode interactions in the 5DLM (6DLM) are still much less complicated than those in global weather models (e.g., Shen et al. 2006a,b) or the model used by Curry et al. (1984), they can be analyzed analytically to trace their impact on solution stability, illustrating the importance of proper selection in the new modes that can effectively increase the degree of nonlinearity. For example, we will discuss how additional nonlinear and damping terms, which are introduced in the 5DLM, can provide negative nonlinear feedback for improving the solution stability. The term "improvement of solution stability" is defined as the disappearance of a positive Lyapunov exponent (LE; e.g., Wolf et al. 1985) or appearance of a stable nontrivial critical point in a generalized LM that has the same system parameters (e.g., the normalized Rayleigh number) as the 3DLM. In a companion paper (B.-W. Shen 2013, unpublished manuscript) with the 6DLM, we further examine the competing impact of an additional heating term as compared to the dissipative and nonlinear terms that are first introduced in the 5DLM. In sections 2a and 2b of this study, we describe the governing equations and present the derivations of the 5DLM. In section 2c, we propose a revised 3D Lorenz model with a "parameterized" term (denoted 3DLMP) that can effectively emulate the impact of the negative nonlinear feedback that is explicitly resolved in the higher-dimensional (5D) LMs. In section 2d, we present the analytical solutions of the critical points in the 5DLM, 3DLM, and 3DLMP. Numerical approaches for the integrations of these models and the calculations of the Lyapunov exponents are discussed in section 2e. In sections 3a and 3b, we use mathematical equations to illustrate the nonlinear feedback loop in the 3DLM and discuss how the feedback loop can be extended with proper selection of new modes in the 5DLM. We then refer to the degree of the extension of the feedback loop, which depends on the number of modes and their hierarchical-scale interactions

TABLE 1. The six modes and their derivatives. Here l and m, representing the horizontal and vertical wavenumbers, are defined as $\pi a/H$ and π/H, respectively. Also, H is the vertical scale of the convection, and a is a ratio of the vertical scale to the horizontal scale. The term $\partial^*/\partial x$ indicates that the outcome is expressed in terms of the selected modes. Mode M_4 is used only in the 6DLM of Shen (2013).

Mode	$\frac{\partial}{\partial x}$	$\frac{\partial^*}{\partial x}$	$\frac{\partial}{\partial z}$
$M_1 = \sqrt{2}\sin(lx)\sin(mz)$	$\sqrt{2}l\cos(lx)\sin(mz)$	lM_2	$\sqrt{2}m\sin(lx)\cos(mz)$
$M_2 = \sqrt{2}\cos(lx)\sin(mz)$	$-\sqrt{2}l\sin(lx)\sin(mz)$	$-lM_1$	$\sqrt{2}m\cos(lx)\cos(mz)$
$M_3 = \sin(2mz)$			$2m\cos(2mz)$
$M_4 = \sqrt{2}\sin(lx)\sin(3mz)$	$\sqrt{2}l\cos(lx)\sin(3mz)$	lM_5	$3\sqrt{2}m\sin(lx)\cos(3mz)$
$M_5 = \sqrt{2}\cos(lx)\sin(3mz)$	$-\sqrt{2}l\sin(lx)\sin(3mz)$	$-lM_4$	$3\sqrt{2}m\cos(lx)\cos(3mz)$
$M_6 = \sin(4mz)$			$4m\cos(4mz)$

(i.e., interconnectivity or interactions of interactions) in the LMs, as the degree of nonlinearity. Then, we present the numerical results of the 3DLM, 5DLM, and 3DLMP in sections 3c and 3d. In section 3e, we discuss the dependence of the solution's stability on the Prandtl number in the (σ, r) space. Conclusions appear at the end.

2. The generalized Lorenz models and numerical methods

a. The governing equations

By assuming 2D (x, z) Boussinesq flow, the following equations were used in Saltzman (1962) and Lorenz (1963a):

$$\frac{\partial}{\partial t}\nabla^2\psi = -J(\psi, \nabla^2\psi) + \nu\nabla^4\psi + g\alpha\frac{\partial\theta}{\partial x}, \tag{1}$$

$$\frac{\partial\theta}{\partial t} = -J(\psi, \theta) + \frac{\Delta T}{H}\frac{\partial\psi}{\partial x} + \kappa\nabla^2\theta, \tag{2}$$

where ψ is the streamfunction that gives $u = -\psi_z$ and $w = \psi_x$, which represent the horizontal and vertical velocity perturbations, respectively, θ is the temperature perturbation, and ΔT is the difference in temperature between the top and bottom boundaries. The constants g, α, ν, and κ denote the acceleration of gravity, the coefficient of thermal expansion, the kinematic viscosity, and the thermal diffusivity (or thermal conductivity), respectively. The Jacobian of two arbitrary functions is defined as

$$J(A, B) = \frac{\partial A}{\partial x}\frac{\partial B}{\partial z} - \frac{\partial A}{\partial z}\frac{\partial B}{\partial x}, \tag{3}$$

$$\nabla^4\psi = \frac{\partial}{\partial x}\left(\nabla^2\frac{\partial\psi}{\partial x}\right) + \frac{\partial}{\partial z}\left(\nabla^2\frac{\partial\psi}{\partial z}\right). \tag{4}$$

For the reader's convenience, we use the same symbols as those in Lorenz (1963a).

b. The 5D Lorenz model

To derive the 5DLM, we use the following five Fourier modes (which are also listed in Table 1):

$$M_1 = \sqrt{2}\sin(lx)\sin(mz),$$
$$M_2 = \sqrt{2}\cos(lx)\sin(mz),$$
$$M_3 = \sin(2mz), \tag{5}$$

$$M_5 = \sqrt{2}\cos(lx)\sin(3mz), \quad M_6 = \sin(4mz), \tag{6}$$

Here l and m are defined as $\pi a/H$ and π/H, representing the horizontal and vertical wavenumbers, respectively, and a is a ratio of the vertical scale of the convection cell to its horizontal scale, (i.e., $a = l/m$). The term H is the domain height, and $2H/a$ represents the domain width. An additional mode $M_4 = \sqrt{2}\sin(lx)\sin(3mz)$ is included to derive the 6DLM, and a comparison of the 6DLM with the 5DLM will be made to examine the impact of an additional heating term (B.-W. Shen 2013, unpublished manuscript). With the five modes in Eqs. (5) and (6), ψ and θ can be represented as

$$\psi = C_1(XM_1), \tag{7}$$

$$\theta = C_2(YM_2 - ZM_3 + Y_1M_5 - Z_1M_6), \tag{8}$$

$$C_1 = \kappa\frac{1+a^2}{a}, \quad C_2 = \frac{\Delta T}{\pi}\frac{R_c}{R_a},$$
$$R_c = \frac{\pi^4}{a^2}(1+a^2)^3, \quad R_a^{-1} = \frac{\nu\kappa}{g\alpha H^3\Delta T}, \tag{9}$$

where C_1 and C_2 are constants, R_a is the Rayleigh number, and R_c is its critical value for the free-slip Rayleigh–Benard problem. With Eqs. (7) and (8), solutions in the 5DLM are represented by the five spatial modes M_1–M_3 and M_5–M_6 and their corresponding time-varying amplitudes (X, Y, Z, Y_1, Z_1), respectively. In the original 3DLM, only three modes (M_1, M_2, M_3) with their amplitudes (X, Y, Z) were used. While the 3DLM and 5DLM have one horizontal wavenumber, they have two and four vertical wavenumbers, respectively. With these modes, the partial differential equations [Eqs. (1) and (2)] can be transformed into ordinary differential equations with only $\partial/\partial t$ retained. Note

that an implicit limitation of this approach is that the nonlinear interactions among the selected modes cannot generate (impact) any new (other) modes that are not preselected, suggesting limited (spatial)-scale interactions. In other words, nonlinear mode–mode interactions are predetermined and limited by the finite number of selected modes. The impact of additional modes (Y_1, Z_1) on the improvement of nonlinear interactions and numerical solutions is discussed in section 3.

To transform Eqs. (1) and (2) into the phase space, a major step is to calculate the nonlinear Jacobian functions. As a result of $J(M_1, M_1) = 0$, there is no explicit term associated with $J(\psi, \nabla^2\psi)$ in the 3DLM or 5DLM. In contrast, the Jacobian term of Eq. (2) can be approximated by four Jacobian terms with selected Fourier modes, which will be analyzed in detail in section 3a. Similarly, we use the five Fourier modes to rewrite the rest of the terms in Eqs. (1) and (2). After collecting the coefficients corresponding to each of the five modes, we obtain the 5DLM with the following five equations:

$$\frac{dX}{d\tau} = -\sigma X + \sigma Y, \tag{10}$$

$$\frac{dY}{d\tau} = -XZ + rX - Y, \tag{11}$$

$$\frac{dZ}{d\tau} = XY - XY_1 - bZ, \tag{12}$$

$$\frac{dY_1}{d\tau} = XZ - 2XZ_1 - d_o Y_1, \tag{13}$$

$$\frac{dZ_1}{d\tau} = 2XY_1 - 4bZ_1. \tag{14}$$

Here $\tau = \kappa(1 + a^2)(\pi/H)^2 t$ (dimensionless time), $\sigma = \nu/\kappa$ (the Prandtl number), $r = R_a/R_c$ (the normalized Rayleigh number or the heating parameter), $b = 4/(1 + a^2)$, and $d_o = (9 + a^2)/(1 + a^2)$. The 3DLM can be obtained from the first three equations of the 5DLM with no inclusion of the nonlinear term XY_1 and are written as

$$\frac{dX}{d\tau} = -\sigma X + \sigma Y, \tag{15}$$

$$\frac{dY}{d\tau} = -XZ + rX - Y, \tag{16}$$

$$\frac{dZ}{d\tau} = XY - bZ. \tag{17}$$

Alternatively, Eqs. (10)–(12) can be viewed as a 3DLM with the feedback processes that are from the two additional modes. In this study, unless otherwise stated, the term "feedback" refers to the nonlinear process that involves the amplitude (Y_1 and/or Z_1) associated with the modes (M_5, M_6), respectively. Thus, the 5DLM may be viewed as a coupled system that consists of a forced dissipative system with low-wavenumber modes [i.e., Eqs. (10)–(12)] and a (nonlinear) dissipative-only system with high-wavenumber modes [i.e., Eqs. (13) and (14)]. Note that the higher-wavenumber mode Y_1 in Eq. (13) [Z_1 in Eq. (14)] has a larger dissipative rate than the lower-wavenumber mode Y in Eq. (11) [Z in Eq. (12)]. As compared to the 5DLM proposed by Roy and Musielak (2007b), our 5DLM applies different mode truncation, has a different feedback term (i.e., XY_1) in $dZ/d\tau$, and does not introduce an additional heating term (which involves r) in $dY_1/d\tau$. Our 5DLM is the lowest-dimensional generalized LM and its simplicity enables us to obtain the analytical solutions, which has never been documented before. In appendix A, we show that the domain-averaged total energy in the 5DLM is conserved in the dissipationless limit and the nonlinear terms may involve the conversion between kinetic and potential energy or between potential energy at different scales. Detailed discussions on the uniqueness of the 5DLM can be found in section 2d and section 3.

c. *A revised 3DLM with parameterized feedback*

The 3DLM contains only two nonlinear terms ($-XZ$ and XY). These two terms form a nonlinear feedback loop, which is discussed in section 3a. A comparison between the 3DLM and Eqs. (10)–(12) of 5DLM shows that the only difference between them is the nonlinear feedback term $-XY_1$, where Y_1 is missing in the 3DLM. One may wonder if it is possible to emulate the impact of $-XY_1$ by representing Y_1 with the existing modes (i.e., resolved modes) of the 3DLM. Indeed, this can be achieved by comparing the solutions of the lower- and higher-dimensional LMs (i.e., the 3DLM and 5DLM), namely, the coarser- and finer-resolution models. Based on the analysis of the critical point solutions in the next section and the calculation of the ratio of Y_1 to X from numerical results (not shown), we assume Y_1 to be linearly proportional to X. As shown in appendix A, that potential energy may cascade from mode M_3 to mode M_6 and dissipate subsequently [e.g., Eqs. (A7) and (A8)], we therefore propose to emulate (or approximate) the feedback processes associated with $-XY_1$ using an eddy dissipation term $-qX^2$, where q is a tunable nonnegative parameter ($q \geq 0$). Mathematically, we can express q as a function of time. However, to illustrate the nature of the negative feedback without the loss of generality, we simply assume q to be a constant. The procedure of emulating the unresolved term XY_1 using the resolved term X^2 is indeed parameterization, per se. Therefore, Eq. (17) [or Eq. (12)] is modified to become

$$\frac{dZ}{d\tau} = XY - qX^2 - bZ. \tag{18}$$

Equations (15), (16), and (18) form the revised 3DLM with the parameterized feedback term. To facilitate the discussions below, the revised 3DLM with a reasonable value of q is referred to as revised 3DLM, revised 3DLMP, or 3DLMP. The choice of q is to improve the solution's stability as well as to produce "reasonable" results, which are discussed in section 3d.

d. Analytical solutions of critical points

Critical points are defined as the solutions to the set of the simultaneous algebraic equations derived from Eqs. (10)–(14) or (15)–(17) with no time-dependent terms (Bender and Orszag 1978). Critical points are also called equilibrium points or fixed points in the literature. Three kinds of critical points are categorized, including a stable node, an unstable node, and a saddle node. The solution of an LM is called a trajectory in the phase space. For a stable (unstable) node, all trajectories converge toward (diverge away from) the critical point. For a saddle node, some trajectories may move toward the critical point, while others may move away from it. A nonlinear system with an unstable (nontrivial) critical point may show a sensitive dependence of solutions on initial conditions and thus are less predictable than the system with only stable critical points. As a trajectory approaches a stable critical point, the solutions, which are normalized or rescaled by the values at a critical point, should eventually become positive (or negative) one. Therefore, the evolution of the differences between the normalized solution and the unity can be a good indicator of whether the solution reaches a steady state. This criterion is potentially useful for examining the time evolution of a system over a wide range of values in the r, as to be illustrated in section 3. To calculate the normalized solution, we need first to solve for the critical point(s) analytically or numerically. It has been challenging to achieve this because of the following. First, in general, it is not easy to obtain the analytical solutions of the critical points in a nonlinear generalized LM containing more equations than the original 3DLM. Second, critical points are usually a function of multiple parameters (such as r and b) and thus cannot be determined numerically prior to time integration. In other words, given a specific set of parameters, (stable) critical points can be obtained only after the completion of the integration that eventually leads to steady-state solutions. However, it still remains challenging to obtain the solutions of unstable critical points numerically. Although the 5DLM contains two additional modes and is indeed more complicated than the 3DLM, its mathematical simplicity with respect to the existing generalized LMs makes it easier to obtain the analytical solutions of the critical points as follows:

$$Z_c = r - 1, \tag{19a}$$

$$Z_{1c} = \frac{-d_o \pm \sqrt{d_o^2 + 4Z_c^2}}{4}, \tag{19b}$$

$$X_c = Y_c = \pm\sqrt{\frac{2bd_oZ_{1c}}{Z_c - 2Z_{1c}}} = \pm\sqrt{b(Z_c + 2Z_{1c})}, \tag{19c}$$

$$Y_{1c} = \frac{X_c}{d_o}(Z_c - 2Z_{1c}), \tag{19d}$$

which can be used to normalize solutions. Note that the sign of Z_{1c} determines whether the solution of X_c is real or imaginary. In the above, only positive Z_{1c} in Eq. (19b) is chosen to have two real roots for X_c. In cases with larger r and comparable domain height and width [namely, $a = O(1)$], we can assume $d_o^2 + 4Z_c^2 \sim 4Z_c^2$, leading to

$$Z_{1c} \sim -d_o/4 + Z_c/2, \tag{20a}$$

$$X_c = Y_c \sim \pm\sqrt{4bZ_{1c}} \sim \pm\sqrt{2bZ_c}, \tag{20b}$$

$$Y_{1c} \sim X_c/2. \tag{20c}$$

The last approximation was used in a simple parameterization scheme in section 2c.

Used as normalization scales in section 3, the nontrivial critical points of the original 3DLM (Lorenz 1963a) are

$$Z_c^{3d} = r - 1, \tag{21a}$$

$$X_c^{3d} = Y_c^{3d} = \pm\sqrt{bZ_c^{3d}}. \tag{21b}$$

When the parameterized feedback term $-qX^2$ is included, the critical points in the revised 3DLM (i.e., 3DLMP) are changed to

$$Z_c^{r3d} = r - 1, \tag{22a}$$

$$X_c^{r3d} = Y_c^{r3d} = \pm\sqrt{\frac{bZ_c^{r3d}}{1-q}}. \tag{22b}$$

Note that while a critical point for Z in the 3DLM, revised 3DLM, and 5DLM has the same mathematical form, the critical points for X and Y are different. A choice of q between 0 and 0.5 leads to $X_c^{3d} \le X_c^{r3d} \le X_c$,

as shown in Eqs. (19c), (21b), and (22b). The differences between X_c^{3d} and X_c^{r3d} can be small when a small q is used, which will be discussed in section 3d.

Based on the previous discussions, one may wonder if a four-dimensional LM (4DLM) can be obtained with additional simplifications. By ignoring Z_1 (i.e., XZ_1) in Eq. (13), the nontrivial critical point solution of X_c for Eqs. (10)–(13) can be obtained: $X_c^2 = -bd_o(r-1)/(r-d_o-1)$. The term X_c^2 becomes negative when $d_o + 1 < r$, and thus X_c has no real root. In addition, the domain-averaged total energy of the 4DLM is not conserved, which is discussed in appendix A. Therefore, the 4DLM is not discussed in this study as a result of the choice with $d_o = 19/3$ and $r > 20$.

e. Numerical approaches

The 3DLM, 3DLMP, and 5DLM are integrated forward in time with the fourth-order Runge–Kutta scheme. Since our main goal is to understand the impact of the additional modes on the representation of the advection of the temperature perturbation and the subsequent nonlinear interaction, we vary the value of r with other parameters kept constant, including $\sigma = 10$, $a = 1/\sqrt{2}$, and $b = 8/3$, as commonly used in previous studies with the 3DLM. The choice of $a = 1/\sqrt{2}$ gives a minimum value for $R_c = 27\pi^4/4$ and $d_o = 19/3$. Note that d only appears in the 5DLM. The dependence of solution stability on σ will be discussed in section 3e. A dimensionless time interval $\Delta\tau$ of 0.0001 is used, and a total number of time steps is 500 000, giving a total dimensionless time τ of 50. A larger τ is used to measure the chaotic behavior of the numerical solutions, as discussed in the next paragraph. [In Figs. 3–6 and 9, the initial value of Y is one ($Y = 1$) and the initial conditions for the rest of the modes (X, Z, Y_1, Z_1) are set to zero.] All of the solutions for the 5DLM, 3DLM, and 3DLMP, unless stated otherwise, are rescaled (or normalized) using the solutions of the critical points in Eqs. (19), (21), and (21), respectively.

To quantitatively evaluate whether the system is chaotic or not, we calculate LE, which is a measure of the average separation speed of nearby trajectories on the critical point. The mathematical definition of the LE (λ_{LE}) is defined as

$$\lambda_{LE} = \mathrm{LE} = \lim_{T\to\infty} \frac{1}{T}\log\left|\frac{\delta\mathbf{s}(T)}{\delta\mathbf{s}(0)}\right|, \tag{23}$$

for a system

$$\frac{ds_i}{d\tau} = f_i(s_1, s_2, \ldots, s_n), \quad i = 1, 2, 3, \ldots, n, \tag{24}$$

where n represents the dimensions of the LM (i.e., number of variables), the integration time $T = N\Delta\tau$, $\mathbf{s}$ is a column vector representing the solution [e.g., $\mathbf{s} = (s_1, s_2, \ldots, s_n)$ and $\mathbf{s} = (X, Y, Z)$ for the 3DLM], and $\mathbf{f}$ is a vector consisting of the terms on the right-hand side in each of the LMs. The value $|\delta\mathbf{s}|$ represents the distance between the perturbed and unperturbed trajectories, and $|\delta\mathbf{s}(0)|$ is an initial distance. Note that to examine the predictability in weather prediction models, a finite-time (FT) LE is calculated (e.g., Nese 1989; Eckhardt and Yao 1993; Kazantsev 1999; Ding and Li 2007; Li and Ding 2011), and it is defined as

$$\lambda_{FTLE}[\mathbf{s}(k\Delta\tau)] = \frac{1}{\Delta\tau}\log\left|\frac{\delta\mathbf{s}[(k+1)\Delta\tau]}{\delta\mathbf{s}(k\Delta\tau)}\right|, \tag{25}$$

which depends on $\Delta\tau$, a starting point (or an initial point), and an initial perturbation. The relationship between the LE and FT LE is shown as follows:

$$\lambda_{LE} = \lim_{N\to\infty}\sum_{k=0}^{N-1}\lambda_{FTLE}[\mathbf{s}(k\Delta\tau)]. \tag{26}$$

Over the past few decades, different numerical schemes have been proposed to calculate $\delta\mathbf{s}$ and thus the LE (e.g., Froyland and Alfsen 1984; Wolf et al. 1985). For example, $\delta\mathbf{s}$ can be calculated by solving the 5DLM and the following equation (e.g., Nese 1989; Eckhardt and Yao 1993):

$$\delta\frac{d\mathbf{s}}{d\tau} = \frac{\partial f_i}{\partial s_j}\delta\mathbf{s}, \quad i, j = 1, 2, 3 \ldots . n. \tag{27}$$

Equation (27) is called the variational equation with additional n^2 equations. In this study, the following two methods are used: 1) the trajectory separation (TS or orbit separation) method (e.g., Sprott 2003) and 2) the Gram–Schmidt reorthonormalization (GSR) procedure (e.g., Wolf et al. 1985; Christiansen and Rugh 1997). The differences between these two schemes are briefly discussed as follows. The TS scheme determines an LE by directly solving Eq. (24) to measure the distance of two trajectories with tiny differences (i.e., 10^{-9} in this study) at the location of the starting points, while the GSR method calculates an LE by simultaneously solving Eqs. (24) and (27), that is, the LM and its variational equation. In both schemes, renormalizations are required during the time integrations. Using the given ICs and a set of parameters in the LMs, the TS scheme calculates the largest LE, and the GSR scheme produces n LEs. Since our interest is to understand whether the system is chaotic with a positive LE, we only analyze the leading (largest) LE with $\Delta\tau = 0.0001$ and $N = 10\,000\,000$,

TABLE 2. The Jacobian functions for the nonlinear interactions of the six modes. Coef indicates the coefficient corresponding to the specific Jacobian function. The crossed-out symbol indicates the negligence of a term that involves the crossed-out term. For example, $\cancel{\cos(2lx)}$ means that any multiplications of the $\cos(2lx)$ are neglected as a result of mode truncation. Mode M_4 is used only in the 6DLM of Shen (2013).

Jacobian	Outcome	Coef	6DLM	5DLM	3DLM
$J(M_1, M_2)$	mlM_3	XY		As in 6DLM	As in 5DLM
$J(M_1, M_3)$	$ml(M_5 - M_2)$	XZ		As in 6DLM	M_5 is missing
$J(M_1, M_5)$	$2mlM_6 - mlM_3$	XY_1	$\cancel{\cos(2lx)}$	As in 6DLM	N/A
$J(M_1, M_6)$	$-2mlM_5$	XZ_1	$\cancel{\sin(5mz)}$	As in 6DLM	N/A
$J(M_4, M_2)$	$2mlM_6 - mlM_3$	X_1Y	$\cancel{\cos(2lx)}$	N/A	N/A
$J(M_4, M_3)$	mlM_2	X_1Z	$\cancel{\sin(5mz)}$	N/A	N/A
$J(M_4, M_5)$	$\cancel{3ml\sin(6mz)}$	X_1Y_1	All missing	N/A	N/A
$J(M_4, M_6)$	$-2mlM_2$	X_1Z_1	$\cancel{\sin(7mz)}$	N/A	N/A
$J(M_1, M_4)$	$\cancel{\propto \sin(2lx)\ldots}$	XX_1	$\cancel{\sin(2lx)}$	N/A	N/A

giving the $\tau = 1000$. To minimize the dependence on ICs, 10 000 ensemble (En = 10 000) runs with the same model configurations but different ICs are performed and an ensemble-averaged LE (eLE) is obtained from the average of the 10 000 LEs. The 10 000 different ICs are produced as Gaussian white noise with the center at the trivial critical point (i.e., with a mean value of zero for the ICs) using a method described by Press et al. (1992). For a given r, it takes approximately 20.5 (10.5) wall-time hours to obtain an eLE with the 5DLM (3DLM). To reduce the wall time to obtain eLEs over a wide range of r, a simple task-level parallelism is implemented to perform parallel calculations using multiple computing processors on National Aeronautics and Space Administration (NASA) supercomputers (e.g., Biswas et al. 2007; Shen et al. 2011). Each of the parallel runs is responsible for the eLE calculation for a given r. The details of the computational issues, the implementation, and further improvement are being documented in a separate paper.

Note that small $\Delta\tau$ and large N and En are used simply because our goal is to understand the long-term-averaged behavior of the solutions of the LMs. Unless stated otherwise, in this study, the eLEs as a function of r are discussed. Here we mainly analyze the results from the TS scheme (in Figs. 7, 8, 10) and use the results with the GSR scheme for verification (in Fig. 7a). To verify the performance of the GSR scheme, its leading eLEs are being used to estimate the Kaplan–Yorke fractal dimension (Kaplan and Yorke 1979). For a given $r = 28$ and $\sigma = 10$, the estimated fractal dimension with the GSR scheme is 2.061 272 08, which is very close to the 2.063 reported in Nese et al. (1987, p. 1957), and close to the 2.062 reported by Professor Sprott (http://sprott.physics.wisc.edu/chaos/lorenzle.htm). Additional experiments indicate that a larger $\Delta\tau$ and smaller N and En could also produce similar results with no impact on the conclusions of this study.

3. Nonlinear feedback of additional modes and their impacts on system stability

In the following sections, we discuss the impact of additional modes on the degree of nonlinearity and solution stability. We analyze the Jacobian term $J(\psi, \theta)$ to illustrate the nonlinear feedback loop of the 3DLM in section 3a and discuss how the feedback loop is extended by the proper selection of the M_5 and M_6 modes in section 3b. Then, we present numerical results from the 5DLM to examine the impact of the nonlinear feedback processes enabled by the two new modes in section 3c. The results of the revised 3DLMP with a parameterized term are analyzed in section 3d to verify the role of the negative feedback in improving solution stability.

a. *The nonlinear feedback loop in the 3DLM*

In this section, we first discuss the characteristics of nonlinearity in the partial differential equation [Eq. (2)], which can be written in terms of Jacobian terms or Fourier models as follows:

$$J(\psi,\theta) = C_1C_2[XYJ(M_1,M_2) - XZJ(M_1,M_3) + XY_1J(M_1,M_5) - XZ_1J(M_1,M_6)] \tag{28}$$

or

$$J(\psi,\theta) = mlC_1C_2(XZM_2 + XYM_3 - XY_1M_3 - XZM_5 + 2XZ_1M_5 + 2XY_1M_6). \tag{29}$$

The outcome for each of the four Jacobian terms on the right-hand side of Eq. (28) is listed in Table 2. Only the first two Jacobian terms are included in the 3DLM. The four nonlinear terms $J(M_1, M_j)$, where $j = 2, 3, 5$, and 6, may involve downscale and/or upscale transfer processes, as described by Eqs. (B2) and (B3) in appendix B, which are briefly summarized. The nonlinear interaction of two wave modes via the Jacobian term can

generate or impact a third wave mode through a downscale (or upscale) transfer process; its subsequent upscale (or downscale) transfer process can provide feedback to the incipient wave mode(s). The downscale and upscale transfer processes form a nonlinear feedback loop, which can be continuously extended as long as new modes could be continuously generated. This suggests that a numerical model should include an infinite number of Fourier modes. However, practically, all of the available numerical models have a finite number of modes and thus the extension of their nonlinear feedback loop is finite (and incomplete). The degree of nonlinearity was previously defined as the degree of mode–mode interactions in the introduction, and it indeed refers to the degree of the extension of the nonlinear feedback loop. We discuss the nonlinear feedback loop of the 3DLM below and its extension in the 5DLM in section 3b.

The degree of nonlinearity is discussed below and is briefly summarized in Fig. 1 where for a given $J(M_1, M_j)$ term, the associated downscale and upscale transfer processes are indicated by a downward arrow and an upward arrow, respectively. In the 3DLM, the nonlinear terms $J(M_1, M_2)$ and $J(M_1, M_3)$ form a feedback loop as a result of the following:

$$J(M_1, M_2) = mlM_3, \tag{30}$$

$$J(M_1, M_3) = -mlM_2. \tag{31}$$

The loop with $M_2 \rightarrow M_3 \rightarrow M_2$ is enabled by the inclusion of the M_3 and is indicated by two pink arrows in Fig. 1. We now illustrate the role of the nonlinear feedback loop in the 3DLM. Without the inclusion of the nonlinear terms $-XZ$ and XY, the 3DLM, that is, Eqs. (15)–(17), reduces to

$$\frac{dX}{d\tau} = -\sigma X + \sigma Y, \tag{32}$$

$$\frac{dY}{d\tau} = rX - Y, \tag{33}$$

$$\frac{dZ}{d\tau} = -bZ. \tag{34}$$

Equations (32) and (33), which are decoupled with Eq. (34), form a forced dissipative system with only linear terms. Equations (32)–(34) also represent the original Lorenz system linearized at the trivial critical point. The system has only a trivial critical point ($X = Y = 0$) and produces unstable normal-mode solutions (i.e., exponentially growing with time) as $r > 1$. While Eq. (33) contains one heating term (rX) and one dissipative term ($-Y$), Eq. (34) has one dissipative term ($-bZ$). Therefore, our

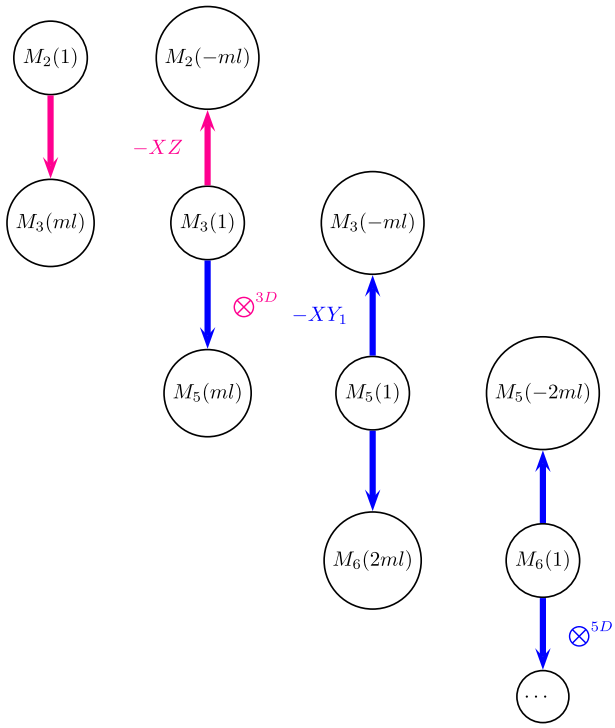

FIG. 1. A schematic diagram of the feedback loop that consists of the downscale and upscale transfer processes associated with $J(M_1, M_j)$, where $j = 2, 3, 5$, or 6. For a given M_j mode, $J(M_1, M_j)$ may lead to a downscale transfer process indicated by a downward arrow and an upscale transfer process indicated by an upward arrow. While scale interactions in the 3DLM forms a feedback loop (pink arrows), additional interactions in the 5DLM extend the feedback loop (blue arrows). The original feedback loop (pink arrows) and extended feedback loops (blue arrows) may be viewed as the main trunk and branches, respectively. A number in parentheses is the coefficient of the specific mode. The $M_3(ml)$ in the leftmost column represents that the M_3 mode with a coefficient of ml is generated or influenced by a downscale transfer process from $J(M_1, M_2)$. The terms $-XZ$ and $-XY_1$, which appear in Eqs. (11) and (12), are associated with the upscale transfer process of the $J(M_1, M_3)$ (by the pink upward arrow) and $J(M_1, M_5)$ (by the blue upward arrow), respectively. The characters $\otimes^{3D}$ and $\otimes^{5D}$ indicate the end of downscale transfer due to mode truncation in the 3DLM and 5DLM, respectively.

analysis indicates that the inclusion of M_3 introduces Eq. (34) and the enabled feedback loop [i.e., Eqs. (30) and (31)] couples Eq. (34) with Eqs. (32) and (33) to form the (nonlinear) 3DLM [Eqs. (15)–(17)] that enables the appearance of convection solutions. From a perspective of total energy conservation, the inclusion of the M_3 mode can help conserve the total energy in the dissipationless limit, which is discussed in appendix A. Mathematically, the feedback loop with the nonlinear terms in Eqs. (16) and (17) leads to the change in the behavior of the system's solutions; the (nonlinear) 3DLM system produces nontrivial critical points, which may be stable (e.g., for $1 < r < 24.74$) or "unstable" (chaotic) (e.g., for

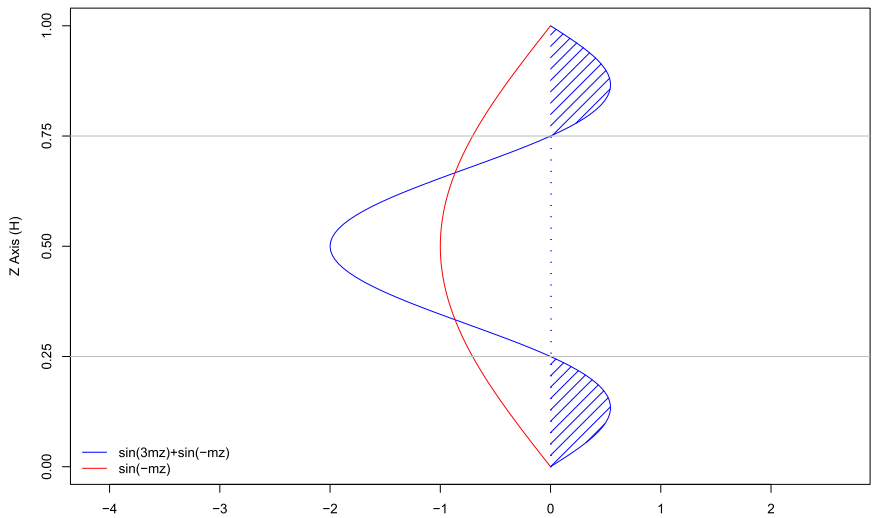

FIG. 2. A comparison between [sin(3mz) + sin($-mz$)] (blue curve) and sin($-mz$) (red curve). The first represents the interaction of M_1 and M_3 via $J(M_1, M_3)$, and the second provides an approximation to $J(M_1, M_3)$ by neglecting sin(3mz) in the original 3DLM. The areas shaded with blue lines indicate opposite phases between these two modes at $0 \le z \le H/4$ and $3H/4 \le z \le H$.

$r > 25$). Note that Eq. (17) has one nonlinear and one dissipative term. Similarly, Eqs. (13) and (14) in the 5DLM, which are introduced by the new modes, contain only nonlinear and dissipative terms (e.g., with no additional heating terms). Their collective impact on the solution stability is examined in sections 3c and 3e. Next, we discuss how the new modes are selected in the 5DLM to extend the feedback loop of the 3DLM.

b. *The extended nonlinear feedback loop in the 5DLM*

Physically, the two modes (M_5 and M_6) with higher vertical wavenumbers are added to improve the presentation of vertical temperature gradients and, therefore, the accuracy of the vertical advection of temperature. From the nonlinear perspective, the inclusion of M_5 is to improve the representation of $J(M_1, M_3)$, a critical nonlinear term in the original 3DLM. This is illustrated as follows. $J(M_1, M_3)$ in the 5DLM is written as

$$\begin{aligned} J(M_1, M_3) &= \sqrt{2}ml\cos(lx)[\sin(3mz) + \sin(-mz)] \\ &= ml(M_5 - M_2), \end{aligned} \tag{35}$$

which is proportional to Eq. (B2) with $(p, q) = (m, 2m)$. Equation (35) indicates the route of the energy transfer to both the M_5 and M_2 modes from $J(M_1, M_3)$, leading to the appearance of $-XZ$ and XZ in Eqs. (11) and (13), respectively, in the 5DLM. More importantly, the interaction of the M_1 and M_5 modes provides feedback to the M_3 mode through

$$J(M_1, M_5) = 2mlM_6 - mlM_3. \tag{36}$$

The above equation, which shares the similarity with Eq. (B3) as $(p, q) = (m, 2m)$, adds the $-XY_1$ term into $dZ/d\tau$ in Eq. (12) for the 5DLM. The processes in Eqs. (35) and (36) extend the (existing) feedback loop (e.g., $M_2 \rightarrow M_3 \rightarrow M_2$) of the 3DLM with a new loop (e.g., $M_3 \rightarrow M_5 \rightarrow M_3$). The former and latter may be viewed as the main trunk and branch, respectively. Note that the term "extension of the nonlinear feedback loop" indicates the linkage between the existing loop and the new loop and thus suggests the importance in the proper selection of new modes. It was reported that the inclusion of new modes could produce additional equations that are not coupled with the 3DLM, leading to a generalized LM with the same stability as the 3DLM [e.g., Eqs. (11)–(16) of Roy and Musielak (2007a)]. In this case, the original nonlinear feedback loop (of the 3DLM) is not extended with the new modes.

Equations (31) and (35) indicate the differences in the representation of the nonlinear $J(M_1, M_3)$ for the 3DLM and 5DLM. The missing M_5 in Eq. (31) is equivalent to replacing the [sin(3mz) + sin($-mz$)] by sin($-mz$). As indicated by a simple comparison between the two terms in Fig. 2, the inclusion of the new mode leads to finer representation of $J(\psi, \theta)$ near the top and bottom boundaries. Specifically, the solutions in Eqs. (31) and (35) have different signs in layers of ($0 < z < H/4$) and ($3H/4 < z < H$), suggesting opposite phases. The differences are presumably related to the rapid changes in the sign of the solutions in the presence of chaos, which, however, is beyond the scope of the present study.

Mathematically, Eqs. (35) and (36) collectively represent a "forcing" term, $J[M_1, J(M_1, M_3)]$, in $d^2Z/d\tau^2$ that

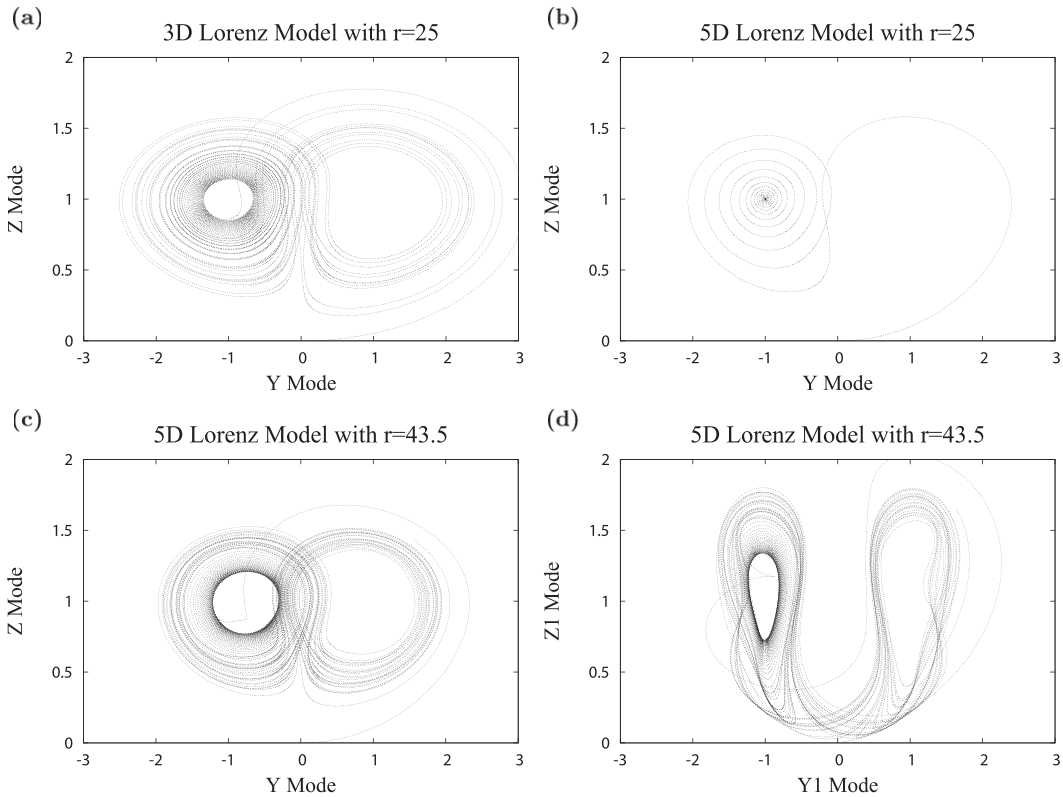

FIG. 3. Phase space plots in the (a) 3DLM and (b)–(d) 5DLM. (a) $(Y/Y_c^{3d}, Z/Z_c^{3d})$ plot with $r = 25$. It shows the Lorenz strange attractors. (b) $(Y/Y_c, Z/Z_c)$ plot with $r = 25$. (c) A $(Y/Y_c, Z/Z_c)$ plot with $r = 43.5$ with strange attractors. (d) $(Y_1/Y_{1c}, Z_1/Z_{1c})$ plot with $r = 43.5$. All of the solutions are normalized by the corresponding critical points, namely, Eq. (21) for the 3DLM and Eq. (19) for the 5DLM.

can be derived by taking the time derivative of Eq. (2). With the inclusion of M_5, $J(M_1, M_5)$ provides not only upscaling feedback to the M_3 mode but also a downscale energy transfer to a smaller-scale wave mode that, in turn, requires the inclusion of the M_6 mode (Fig. 1; Table 2). As discussed in appendix A, the M_6 mode is required to conserve the total energy in the dissipationless limit. The term XY_1 is responsible for the transfer of the domain-averaged potential energy at different scales (between the M_3 and M_6 modes). The feedback loop is further extended to $M_5 \rightarrow M_6 \rightarrow M_5$ through $J(M_1, M_5)$ and $J(M_1, M_6)$. In summary, while the inclusion of M_3 forms a feedback loop by introducing Eq. (17) in the 3DLM, the inclusion of M_5 and M_6 extends the feedback loop by introducing Eqs. (13) and (14) where additional dissipative terms are included. In the next section, we examine whether the feedback of the aforementioned nonlinear processes is positive or negative and show that the $-XY_1$ term can provide the negative feedback to stabilize solutions.

c. *Numerical results of the 5DLM*

Figure 3 shows the normalized solutions of (Y, Z) and (Y_1, Z_1) using the 3DLM and 5DLM with three different values of r. The scales for normalization are the critical points (e.g., Y_c and Z_c) as defined in Eqs. (19) and (21) for the 5DLM and 3DLM, respectively. As first shown in Lorenz (1963a), when the 3D system (in the 3DLM) becomes chaotic at a large r ($r > r_c$, $r_c = 24.74$), the solution never reaches a steady state but oscillates irregularly with time around the nontrivial critical points. This feature can be seen in Fig. 3a from the 3DLM with $r = 25$. It has been shown that the solution is sensitive to initial conditions, which are referred to as the butterfly effect (of the first kind). As compared to the 3DLM, the 5DLM with the same r value of 25 produces a steady-state solution, as indicated by the converged trajectory that approaches a critical point at $(Y/Y_c, Z/Z_c) = (-1, 1)$ in Fig. 3b. The 5DLM continues to generate steady-state solutions until r is beyond 43 (which will be discussed in Fig. 7). For an r value of 43.5, the 5DLM produces a chaotic solution with a butterfly pattern in the Y–Z space (Fig. 3c). The corresponding solutions for Y_1 and Z_1 are shown in Fig. 3d and have low values when Y rapidly changes its signs.

Numerical results that display temporal fluctuations near the critical points are analyzed in Figs. 4 and 5. For

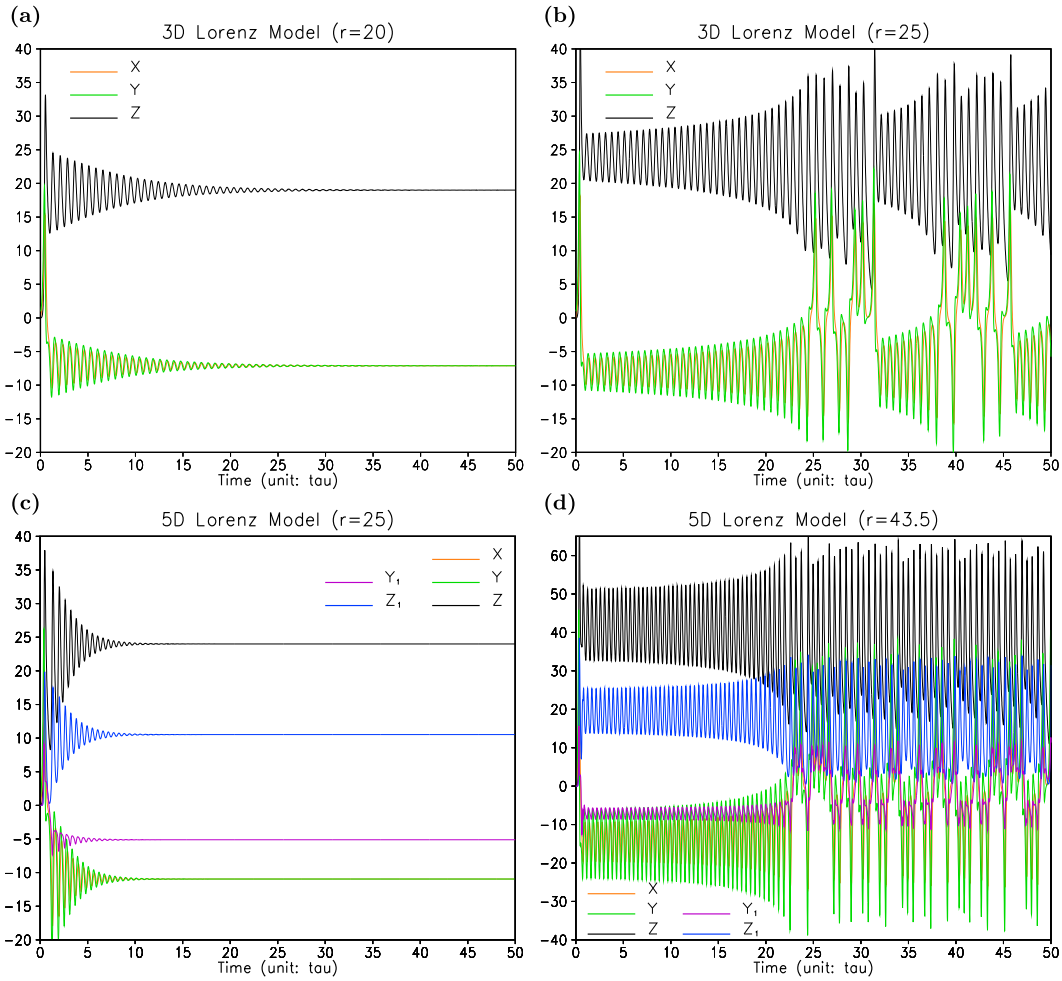

FIG. 4. Time series plots for the (a),(b) 3DLM and (c),(d) 5DLM. The X, Y, and Z plots are in orange, green, and black, respectively. The Y_1 and Z_1 plots are in purple and blue, respectively. The three modes in the 3DLM with (a) $r = 20$ and (b) $r = 25$. The five modes in the 5DLM with (c) $r = 25$ and (d) $r = 43.5$.

stable cases in both the 3DLM and 5DLM (Figs. 4a,c), the solutions oscillate at small time scales and their envelopes decay at large time scales. The decay rate that leads to steady states is larger in the 5DLM than in the 3DLM. For chaotic cases shown in Figs. 4b and 4d, from the 3DLM with $r = 25$ to the 5DLM with $r = 43.5$, respectively, the solutions oscillate in the beginning and gradually grow with time. Chaos appears subsequently; its onset can be identified by rapid changes in the signs of X (or Y).

By calculating the numerical solutions of the 5DLM over a wide range of r and normalizing them using the corresponding critical points in Eq. (19), we show that the r–time diagram of the normalized solutions is useful in displaying stable and chaotic regions, providing a qualitative method of determining the r_c for the onset of chaos. In Fig. 5 where (Z/Z_c, Z_1/Z_{1c}, $-Y/Y_c$, and $-Y_1/Y_{1c}$) are shown, white areas display the normalized values of 1 ± 0.01. For $r = 25$–43, the appearance of stable critical points is indicated by the white areas with a sufficient long period of time. In contrast, a chaotic regime can be identified as $r > r_c$ (where $r_c \sim 43$) by rapid changes in both the sign and magnitude of the normalized solutions. This critical value is consistent with the analysis of the Lyapunov exponent (discussed later with Fig. 7b). Other than the above, this figure is able to monitor the transient processes and suggests a longer time for solutions to become steady (chaotic) when r gets closer to r_c, consistent with the analysis of the eLEs that are close to zero as $r \sim r_c$.

To examine the improved stability of the solutions in the 5DLM, we analyze the time evolution of each term on the right-hand side of Eqs. (10)–(12). Results from Eq. (12) are compared with those from Eq. (17) to illustrate the major difference between the 5DLM and

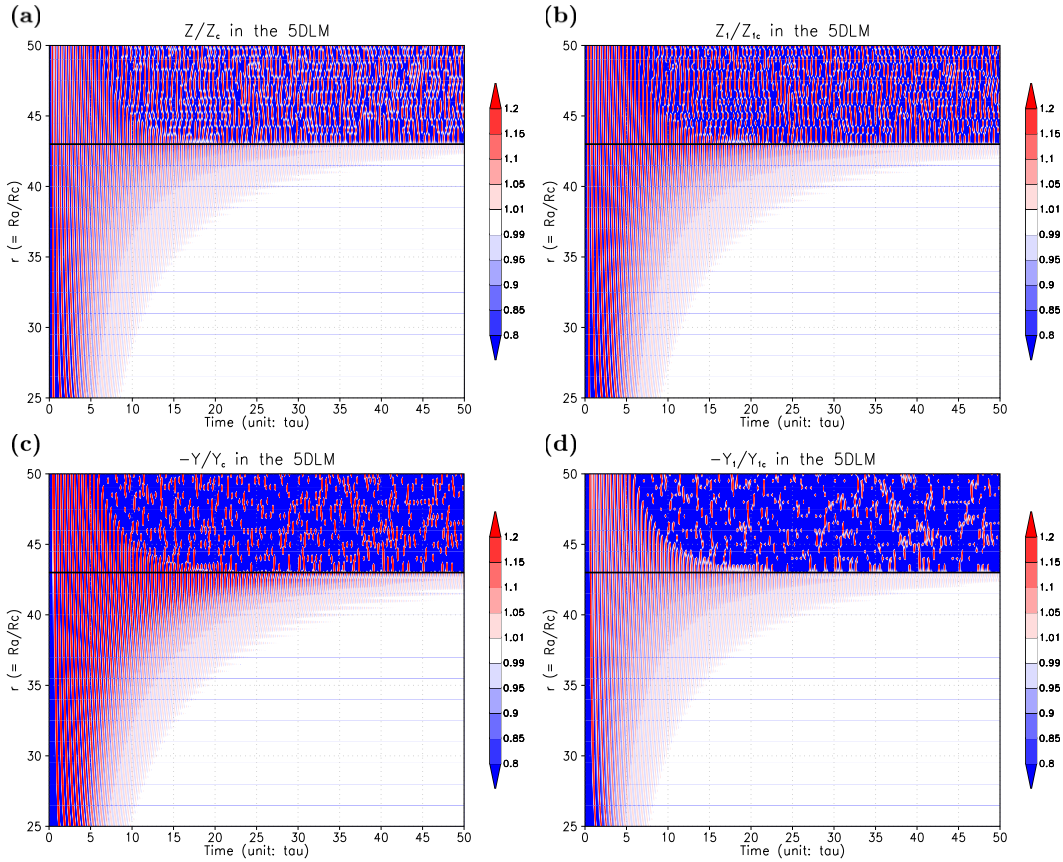

FIG. 5. The r–time diagram of the normalized numerical solutions from the 5DLM. The term r ranges from 25 to 50 with $\Delta r = 0.5$. (a) Z/Z_c, (b) Z_1/Z_{1c}, (c) $-Y/Y_c$, and (d) $-Y_1/Y_{1c}$. The terms Z_c, Z_{1c}, Y_c, and Y_{1c} are defined in Eqs. (19a)–(19d), respectively. The black line indicates the constant value of $r = 43$, which is close to $r_c = 42.9$ for the 5DLM.

3DLM. For a stable case in the 3DLM (e.g., $r = 20$ in Fig. 6a), a steady-state solution exists in association with a balance between the nonlinear term (XY) and the dissipative term (bZ). However, at a large r (e.g., $r = 25$ in Fig. 6b), both of the terms evolve with time at a different growth rate and the solutions appear chaotic. The analysis seemingly supports the understanding that the source of chaos is the nonlinearity, as XY appears as a forcing term with respect to the other term bZ for the M_3 mode in Eq. (17). However, by contrast, the 5DLM using the same normalized Rayleigh number ($r = 25$) produces a steady-state solution that corresponds to the balanced state achieved by the three terms XY, bZ, and XY_1 (Fig. 6c). The second nonlinear term (XY_1) has a magnitude comparable to bZ but is missing in the 3DLM. A similar balanced state can be found in the case with $r = 35$ (Fig. 6d). The comparison between Figs. 6b and 6c suggests the importance of XY_1 in stabilizing the solution with $r = 25$, indicating the importance of an increased degree of nonlinearity. As discussed earlier, the feedback of XY_1 to the $dZ/d\tau$ for the M_3 mode [Eq. (12)] can be mathematically illustrated using a pair of Jacobian functions, $J(M_1, M_3)$ and $J(M_1, M_5)$, depicting the nonlinear processes of downscale transfer and subsequent upscale transfer that extend the feedback loop. From a macroscopic view discussed in appendix A, XY is responsible for the transfer of the domain-averaged kinetic energy and potential energy; XY_1 is responsible for the transfer of the domain-averaged potential energy at different scales, which provides a path for dissipation via the $4bZ_1$ term in Eq. (14).

To quantitatively measure the degree of chaotic responses in the LMs with the goal of understanding the system's predictability, we calculate the eLE using the TS and GSR numerical methods that were discussed in section 2e. Figure 7a shows the eLEs of the 3DLM and 5DLM as a function of r with $20 \leq r \leq 120$ and an increment of one ($\Delta r = 1$), while Fig. 7b shows the eLEs of the 5DLM with $35 \leq r \leq 50$ and $\Delta r = 0.1$. For the 3DLM, the eLEs using the TS scheme, as shown in a pink curve, suggest the appearance of chaos as $r > r_c$, and r_c is approximately 23.7. This r_c is slightly smaller than the

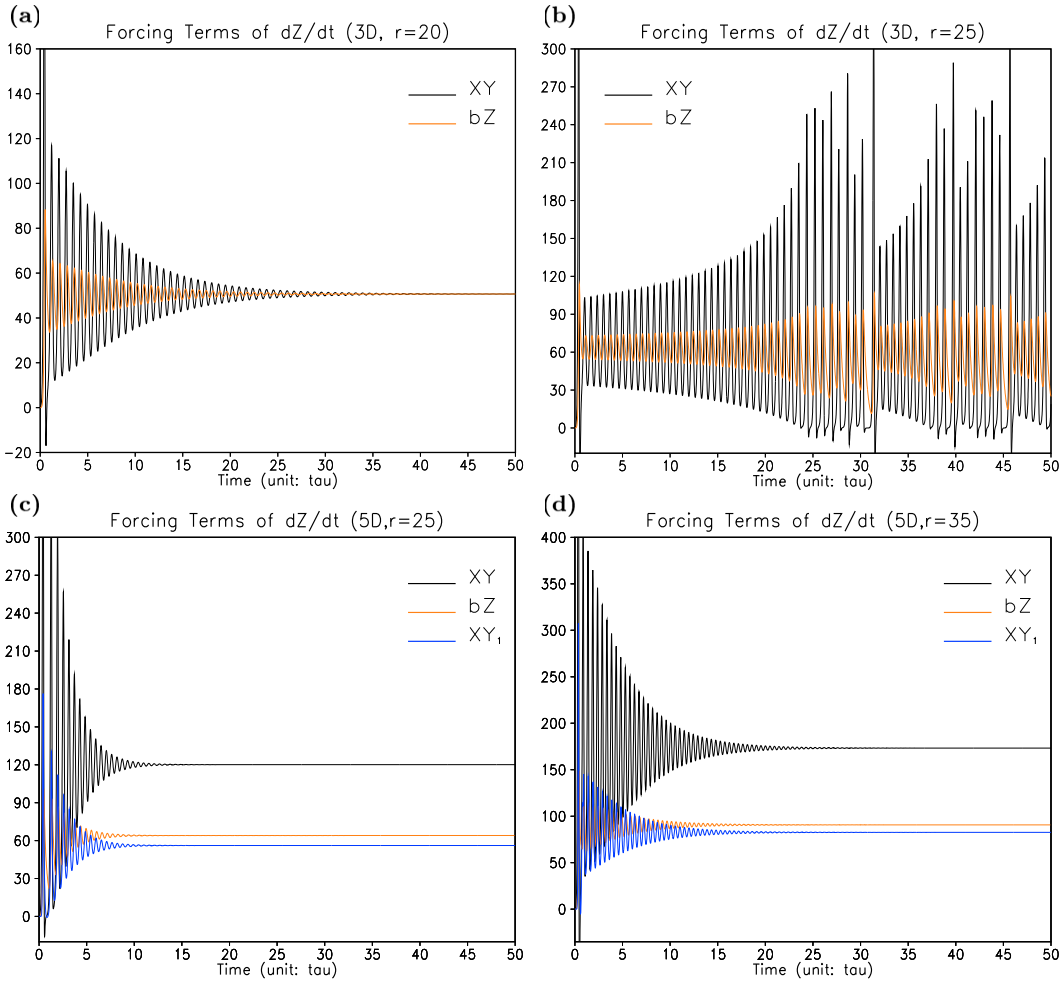

FIG. 6. Forcing terms of $dZ/d\tau$, which are from Eq. (17) of the 3DLM and Eq. (12) of the 5DLM. Results from the 3DLM with (a) $r = 20$ and (b) $r = 25$. Results from the 5DLM with (c) $r = 25$ and (d) $r = 35$. The black and orange lines represent XY and bZ, respectively, while the blue line represents XY_1. In the 3DLM, XY and bZ are balanced to reach a steady state. In the 5DLM, the additional term XY_1 is required to reach a steady state.

(linear) theoretical value of 24.74 proposed by Lorenz (1963a) using the stability analysis of the linearized 3DLM. Note that the accuracy of the r_c depends on many factors, including the values of the system's parameters (e.g., σ, b, and/or d_o), different initial conditions, numerical schemes, and so on. As our goal is to illustrate the (negative) nonlinear feedback associated with the new modes in the generalized LM, we made no attempt at searching for a precise r_c. We use $\Delta r = 0.1$ to identify the r_c, which is defined as the lowest value of r when the eLE becomes positive from negative. In addition to the transition from stable regions (eLEs < 0) to chaotic regions (eLEs > 0), two of the so-called window regions where the LEs are nearly zero can be identified in the vicinity of $r = 93$ and $r = 100$ in the pink curve. The results of the 3DLM, which display a relatively smaller r_c and indicate the appearance of windows, are in good agreement with previous studies [e.g., Fig. 1 of Froyland and Alfsen (1984)]. To understand the sensitivity of the eLE calculations to a specific scheme, a comparison of the eLEs using the TS procedure and GSR scheme (e.g., the orange circle in Fig. 7a) was made, showing insignificant differences except near the window regions (e.g., the green curve in Fig. 7a).

As compared to the 3DLM, the eLEs of the 5DLM (the black curve in Figs. 7a and 7b) indicate the following: (i) that a larger r ($r_c \sim 42.9$) is required for the onset of the chaos; (ii) that one window exists but appears at a slightly larger r (i.e., $r = 107$); and (iii) that eLEs are comparable to the corresponding ones of 3DLM for $44 < r < 80$ and display large differences when $r < 44$ and $r > 80$ (e.g., near window regions).

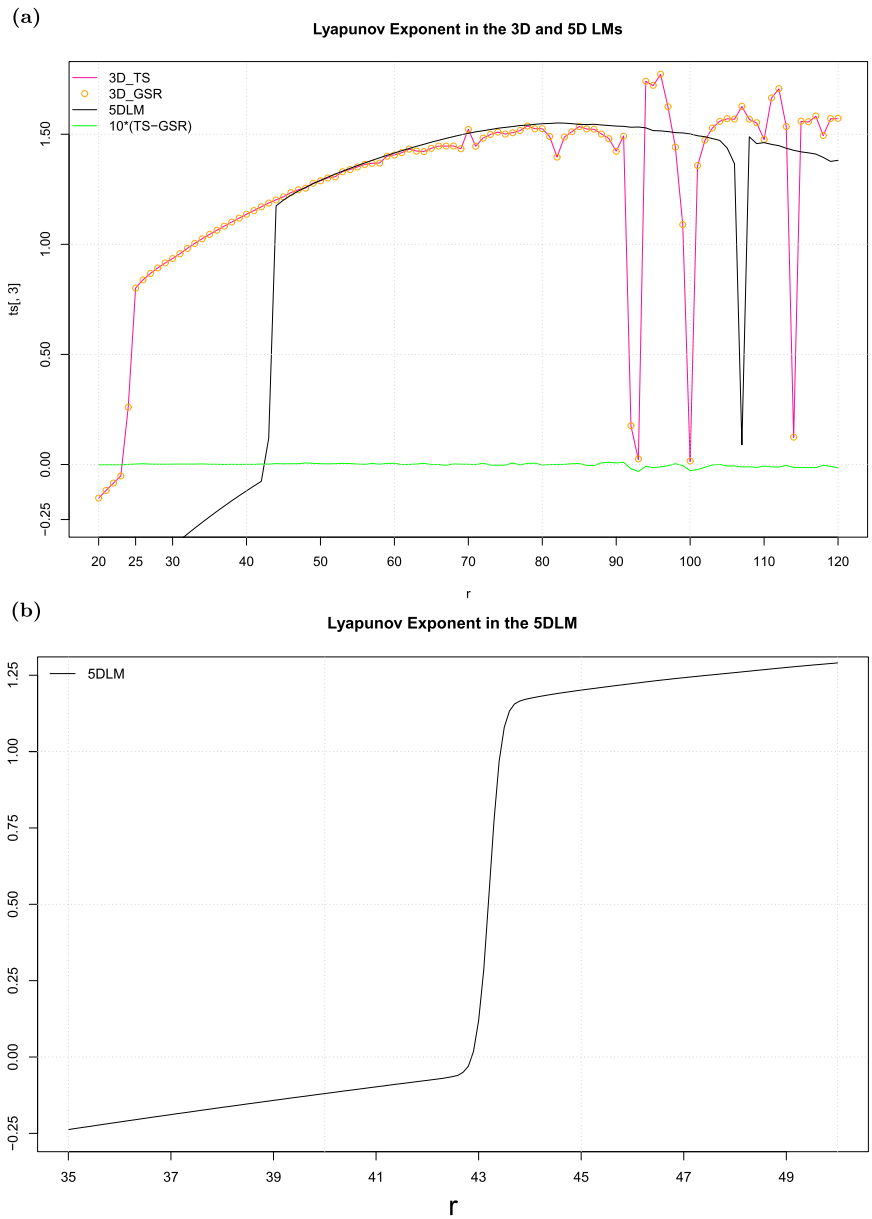

FIG. 7. The largest eLEs as a function of r in different LMs. (a) The eLEs of the 3DLM with $\Delta r = 1$ using different numerical schemes, including the TS scheme (pink) and the GSR procedure (orange). The green line represents the 5-times differences of the results from the two schemes, and the black line indicates the eLEs of the 5DLM. (b) The eLEs with $\Delta r = 0.1$ for the 5DLM. The appearance of chaotic solutions is indicated by positive eLEs. Note that the theoretical critical value of r for the onset of chaos in the original 3DLM is 24.74.

d. Results of the revised 3DLM

The previous discussions indicated that the XY_1 plays a role in stabilizing the solutions in the 5DLM with $25 \leq r \leq 40$, and the XY_1 is the only difference between the first three equations of the 5DLM [Eqs. (10)–(12)] and the 3DLM [Eqs. (15)–(17)]. In section 2c, we proposed to emulate the XY_1 using qX^2 with a tunable parameter q in the revised 3DLM, as shown in Eqs. (15), (16), and (18). The range of q within 0–0.5 can be roughly estimated by the following relation $Y_c^{3d} \leq Y_c^{r3d} \leq Y_c$, which represents the analytical solutions of the critical point Y [e.g., Eqs. (21b), (22b), and (19c)] in the 3DLM, 3DLMP, and 5DLM, respectively. To pin down the range of q that can

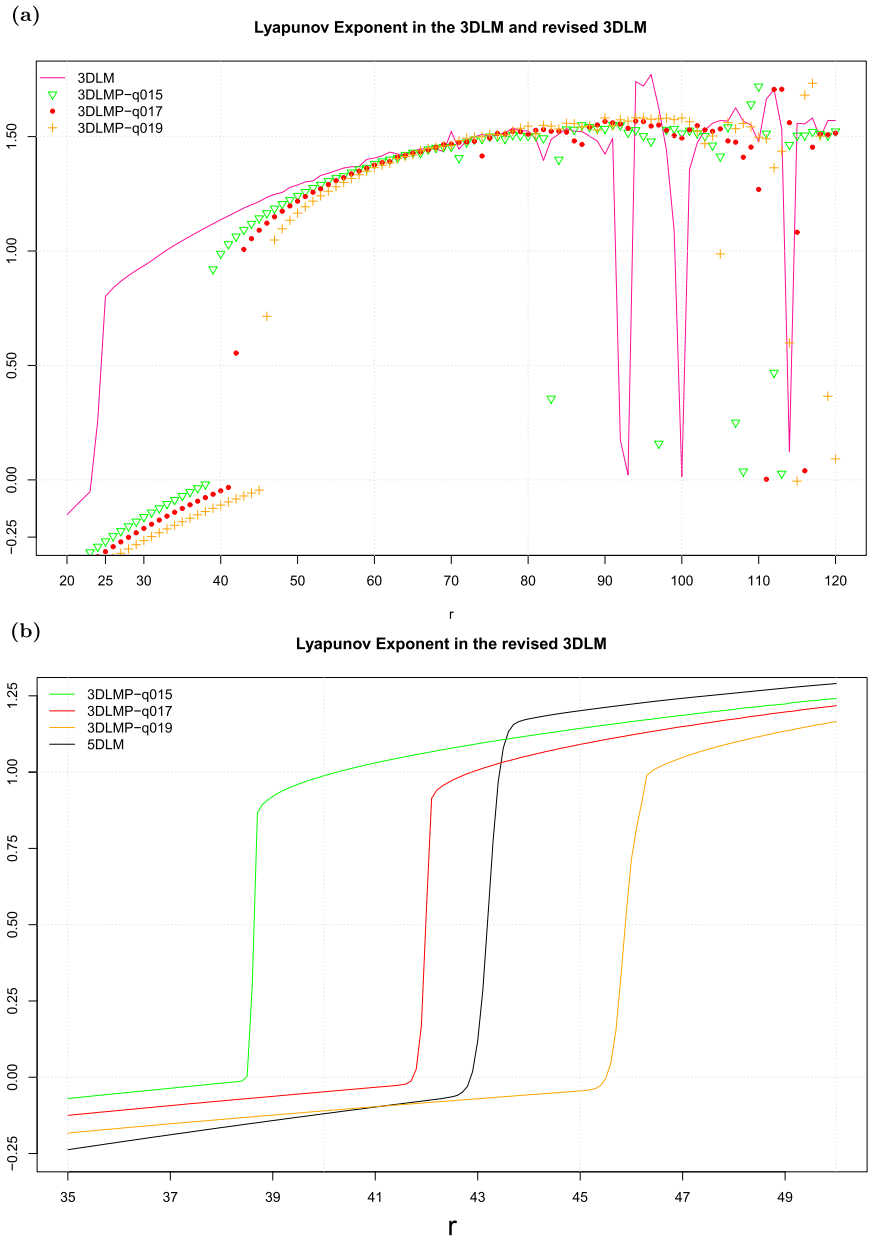

FIG. 8. As in Fig. 7, but for 3DLMP with $q = 0.15$ (green), 0.17 (red), or 0.19 (orange).

effectively provide similar negative feedback, we conduct a limited number of runs using selected values of q. The eLEs of four runs with $q = 0.15, 0.17, 0.19$, and 0.36 are discussed below. For the case with $q = 0.36$, eLEs over the range of $r = 20$–120 are negative and thus suggest stable solutions (not shown). However, its critical point deviates from the corresponding one of the 3DLM by approximately 25% as a result of the relation $X_c^{\mathrm{r3d}}/X_c^{\mathrm{3d}} = \pm\sqrt{1/(1-q)} = \pm 1.25$ [see Eqs. (21b) and (22b)]. Unless stated otherwise, we mainly discuss the revised 3DLM with $q = 0.15, 0.17$, or 0.19 in the following. Figures 8a and 8b show the eLEs of the three cases for $20 \le r \le 120$ and $35 \le r \le 50$, respectively. Each of these cases displays a transition region between $38 < r < 46$, where the eLE turns from negative to positive (Fig. 8a). As compared to the original 3DLM, the transition regions for the three cases with the revised 3DLMP appear at a larger r. Within these transition regions, critical numbers for the onset of chaos can be determined as 38.5, 41.8, and 45.6 for cases with $q = 0.15, 0.17$, and 0.19, respectively (as shown Fig. 8b). For $50 \le r \le 80$, the eLEs of the revised 3DLMPs are comparable to those of the 3DLM (Fig. 8a).

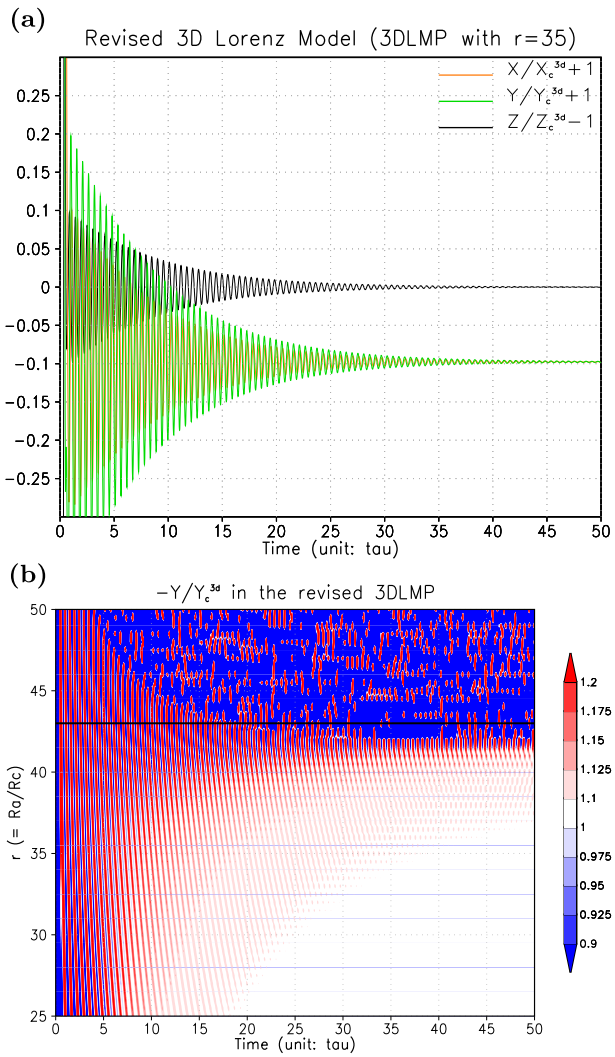

FIG. 9. (a) Time series plots for the revised 3DLMP with $r = 35$ and $q = 0.17$. The orange, green, and black lines show $X/X_c^{3d} + 1$, $Y/Y_c^{3d} + 1$, and $Z_c^{3d} - 1$, respectively. (b) The r–time diagram of the numerical solution $-Y/Y_c^{3d}$ from the revised 3DLMP with a parameterized feedback term ($-qX^2$). The term r ranges from 25 to 50 with $\Delta r = 0.5$. The terms X_c^{3d}, Y_c^{3d}, and Z_c^{3d} are the critical points in the original 3DLM [e.g., Eq. (21)]. The black line indicates the constant value of $r = 43$.

Among these three runs, the case for $q = 0.17$ provides the most comparable results to those of the 5DLM. This case is further analyzed below.

In addition to the long-term-averaged behavior of the solutions represented by the eLEs, we examine the time evolution of the solutions (X, Y, Z) from the revised 3DLM, normalized by the critical points of the original 3DLM [Eq. (21)]. Figure 9a displays the normalized solutions for the case using $r = 35$ and $q = 0.17$ that initially oscillate and later approach a steady state after $\tau = 40$. The steady-state solutions of the nondimensional X/X_c^{3d} and Y/Y_c^{3d} are approximately -1.098, consistent with the calculation using the relation $X_c^{r3d}/X_c^{3d} = \pm\sqrt{1/(1-q)}$. Figure 9b shows the r–time diagram of the normalized solution ($-Y/Y_c^{3d}$) when $25 \le r \le 50$. Areas shaded in white display the normalized solutions between 1 and 1.1 and suggest steady-stage solutions as $r < 40$ with a maximum deviation of 10% from the critical point Y_c^{3d} of the 3DLM.

The above experiments suggested that although the 3DLM becomes chaotic at $25 \le r \le 40$, an additional nonlinear dissipative term that emulates the negative feedback, explicitly resolved in a higher-dimensional (5D) LM, can effectively and realistically stabilize the solutions of the revised 3DLM, leading to a (stable) steady-state solution. Using a given set of system parameters, the critical points (steady-state solutions) in a revised 3DLMP are not exactly the same as those in the original 3DLM. However, the differences between the former and the latter can be remained within 10% if a value of q is properly selected (i.e., $q \le 0.19$).

e. Stability analysis in the (σ, r) space

The previous sections discussed the stability problem by varying r. Here we examine the dependence of solution stability on σ and address the question of whether the 5DLM still requires a larger r for the onset of chaos when different values of σ are used. Although a task-level parallelism was implemented in the schemes for the eLE calculation, it is still computationally intensive for obtaining eLEs over a wide range of values for both σ and r (i.e., $5 \le \sigma \le 25$, $20 \le r \le 50$). Therefore, to achieve our goal efficiently, we begin with the stability analysis of the linearized LMs at a nontrivial critical point and conduct the eLE analysis using selected values of σ. The former is to examine the local predictability, while the latter is to give a measure of the total predictability of the system.

Numerical procedures for the local (or linear) stability analysis in the (σ, r) space are discussed in appendix C and briefly summarized as follows. To perform a stability analysis of the 3DLM, 3DLMP, or 5DLM, we linearize each of these LMs with respect to one of its nontrivial critical points [e.g., Eqs. (C2)–(C6)], obtain its characteristic or eigensystem [i.e., Eq. (C8)], and solve for their eigenvalues. The analytical solutions of critical points for the 5DLM [Eq. (19)], 3DLM [Eq. (21)], and revised 3DLMP [Eq. (22)] are used for the analysis. An eigenvalue λ can be a real or complex number, and its real part is denoted $\mathrm{Re}(\lambda)$. The appearance of a positive $\mathrm{Re}(\lambda)$ suggests an unstable solution near the critical point. In the following, we examine the solution stability by checking whether the largest $\mathrm{Re}(\lambda)$ is positive or negative.

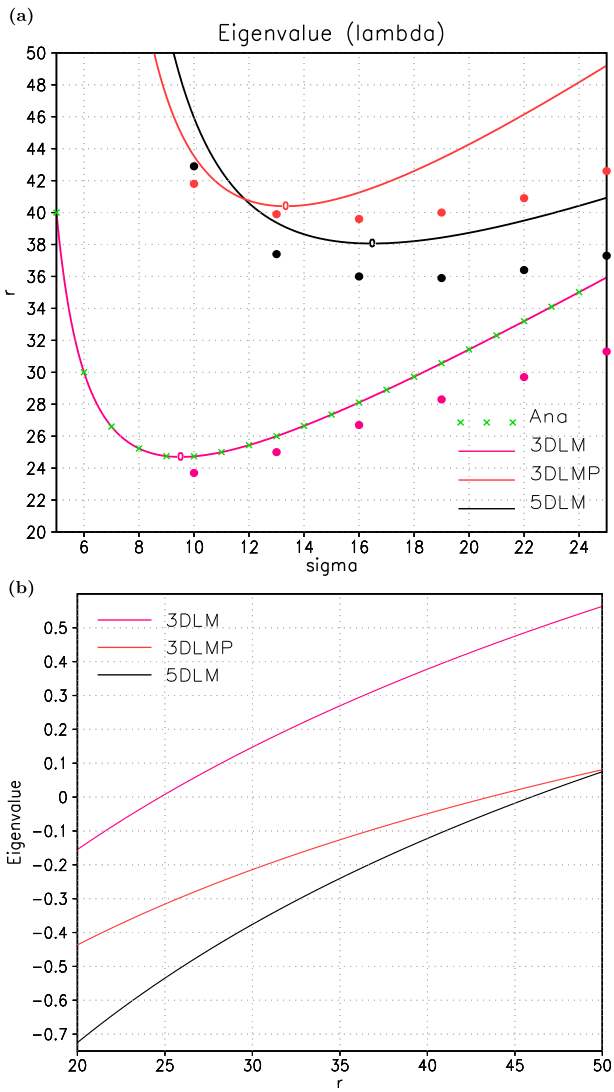

FIG. 10. Stability analysis of the linearized Lorenz models with $\Delta\sigma = 0.01$ and $\Delta r = 0.01$. (a) The leading eigenvalue $\mathrm{Re}(\lambda)$ as a function of σ and r. The pink, red, and black lines indicate a constant contour of $\mathrm{Re}(\lambda) = 0$ for the linearized 3DLM, 3DLMP, and 5DLM, respectively. The solid circles with the same color scheme indicate r_c determined by the eLEs analysis with $\Delta r = 0.1$ in the corresponding nonlinear LM. The green multiplication sign shows the relation $r = \sigma(\sigma + b + 3)/(\sigma - b - 1)$ for $\lambda = 0$ in the linearized 3DLM. (b) $\mathrm{Re}(\lambda)$ as a function of r and a given $\sigma = 10$ for 3DLM (pink), 3DLMP (red), and 5DLM (black). It shows that the critical value of r with $\mathrm{Re}(\lambda) = 0$ is 24.74, 43.54, and 45.94 for the linearized 3DLM, 3DLMP, and 5DLM, respectively.

Figure 10a shows the contour lines of the $\mathrm{Re}(\lambda) = 0$ in the (σ, r) space, each of which describes the critical value r_c^l as a function of σ, where the superscript l indicates the local (or linear) analysis. The pink, red, and black lines show the contour lines of $\mathrm{Re}(\lambda) = 0$ for the 3DLM, 3DLMP, and 5DLM, respectively. Solid circles with the same color scheme indicate the r_c determined using the eLE analysis, as discussed in the next paragraph. The contour line of $\mathrm{Re}(\lambda) = 0$ for the 3DLM is identical to the curve describing the relation $r = \sigma(\sigma + b + 3)/(\sigma - b - 1)$, which was solved analytically to meet $\lambda = 0$ by Lorenz (1963a) (as shown with green multiplication signs in Fig. 10a). Following each of these contour lines in the direction of the increasing σ, its right (left)-hand side contains areas with negative (positive) values of $\mathrm{Re}(\lambda)$, suggesting stable (unstable) solutions. In general, given a fixed σ in each of these LMs, the larger the value of r is, the larger $\mathrm{Re}(\lambda)$ is (e.g., Fig. 10b). Thus, unstable solutions $[\mathrm{Re}(\lambda) > 0]$ appear as $r_c^l < r$. When $\sigma = 10$, the r_c^l values for the 3DLM, 3DLMP, and 5DLM are 24.74, 43.54, and 45.94, respectively (Fig. 10b and Table 3). As compared to the eLE analysis in the previous sections, the linear stability analysis produces comparable but slightly larger critical values. Such a feature was previously documented using the 3DLM by Froyland and Alfsen (1984).

In realizing the stability dependence on σ from the linear analysis, we perform additional eLE calculations using our LMs with $\sigma = 13, 16, 19, 22$, and 25 and plot the r_c values as solid circles. In each of the selected runs, the eLE analysis produces a slightly smaller critical value with respect to the linear stability analysis, that is, $r_c < r_c^l$, as shown in Fig. 10a. As σ increases from 10, the tendency of the increasing r_c in the 3DLM could be seen in both of the linear and eLE analyses (as shown with pink lines and pink solid circles). By comparison, the linear analysis on the revised 3DLMP and 5DLM shows information that r_c first decreases and then increases, and the eLE analysis produces a similar tendency. It is clearly shown in Fig. 10a that when a σ is given (e.g., over the range 5–25), the 5DLM (and 3DLMP) requires a larger r for the onset of chaos than the 3DLM, suggesting improved stability over a wide range of σ.

4. Concluding remarks

In this study, we derived the generalized 5D Lorenz model (LM) to investigate the impact of two higher-wavenumber modes on the numerical predictability. The domain-averaged total energy of the 5DLM is conserved in the dissipationless limit. Distinct from other studies with generalized LMs, we provided physical justification for the choices of additional modes that can improve solution stability and focused on the interpretation of the nonlinear-scale interactions (i.e., increased degree of nonlinearity) enabled by these additional modes. We first illustrated the nonlinear feedback loop in the 3DLM and emphasized the importance of properly selecting new modes to extend the feedback loop and thus improving the degree of nonlinearity in the 5DLM. By comparing

TABLE 3. Numerical experiments with different Lorenz models. The column "$=q=$" indicates additional information in the equations. The column "Figures" lists the figures that include the solutions from each of the Lorenz models. The r_c and r_c^l columns are determined based on the eLEs analysis and linear stability analysis, respectively. Solutions may be rescaled using the equation in the "Scaling factors" column. For the 3DLM, the ensemble-averaged LE is 1.2×10^{-2} at $r = 23.7$ and becomes 0.26 at $r = 24$.

Case ID	Equations	$=q=$	Figures	r_c	r_c^l	Scaling factors
3DLM	Eqs. (15)–(17)	N/A	Figs. 3, 4, 6–8, and 10	23.7	24.74	Eq. (21)
3DLMP	Eqs. (15), (16), and (18)	$q = 0.17$	Figs. 8–10	41.8	43.54	Eq. (21)
5DLM	Eqs. (10)–(14)	N/A	Figs. 3–8 and 10	42.9	45.94	Eq. (19)

with other generalized LMs, we found that the 5DLM might serve as the lowest-order generalized LM with increased system stability. The inclusion of new modes introduces both nonlinear terms and dissipative terms that have collective impact on the increase of solution stability. The additional nonlinear terms are mainly associated with the improved vertical advection of temperature. The mathematical simplicity of the 5DLM with respect to existing generalized LMs makes it easier to obtain the analytical solutions of its critical points, identify the major feedback process and its role in the solutions' stability of the generalized LMs (e.g., 5DLM and 6DLM), and perform (linear) local stability analysis near the critical points over a wide range of parameters (σ, r). The analyses of both local stability and ensemble-averaged Lyapunov exponents (eLEs) show that the 5DLM requires a larger normalized Rayleigh number r for the appearance of chaotic solutions than the 3DLM. While Lorenz demonstrated the association of the nonlinearity with the existence of the nontrivial critical points and strange attractors in the 3DLM, we emphasized the importance of the nonlinearity in both producing new modes and enabling subsequent negative feedback to improve solution stability. More details are given below.

Through the mathematical analysis of the 3DLM, we discussed the feedback loop that includes the nonlinear terms $J(M_1, M_2)$ and $J(M_1, M_3)$ [Eqs. (30) and (31)]. The inclusion of the M_3 mode in the 3DLM enables the appearance of the stable nontrivial critical points when $1 \leq r < 24.74$ but leads to chaotic solutions when $r > 24.74$. In comparison, the inclusion of the M_5 mode in the 5DLM can improve the representation of $J(M_1, M_3)$ by enabling a downscale transfer process and provide feedback to the M_3 mode via an upscale transfer process $J(M_1, M_5)$, which adds the $-XY_1$ term in $dZ/d\tau$ [Eq. (12)]. Therefore, the nonlinear loop is extended through the Jacobian terms $J(M_1, M_3)$ and $J(M_1, M_5)$ [Eqs. (35) and (36)] and is further extended through $J(M_1, M_5)$ and $J(M_1, M_6)$ in the 5DLM, as shown in Fig. 1. Based on the eLE calculations, the critical value r_c for the 5DLM with $\sigma = 10$ is approximately 42.9. The r_c value of the 5DLM is comparable to the one determined by the local stability analysis of the linearized 5DLM that gives 45.94. Both the eLE analysis and the local (or linear) stability analysis suggest that the 5DLM still produces stable steady-state solutions when r ranges from 25 to 42, while the solution of the 3DLM becomes chaotic.

To understand the differences in the predictability between the 3DLM and 5DLM, the competing impact of the nonlinear term XY_1 against other nonlinear and dissipation terms was illustrated with the use of Eq. (12) $dZ/d\tau = XY - XY_1 - bZ$. While the first nonlinear term (XY) and the linear term (bZ) act as a forcing term and dissipative term, respectively, the second nonlinear term (XY_1) may work as an additional dissipative term. Therefore, chaotic responses that appear in the 3DLM can be suppressed further by the additional modes in the 5DLM, producing stable solutions such as $1 \leq r < 42.9$. However, we would like to emphasize that the negative feedback by the term $-XY_1$ comes from the collective effects of the nonlinear and dissipative terms associated with the new modes and that it is not trivial to separate them. A macroscopic view suggests that XY_1 enables the transfer of domain-averaged potential energy at different scales, which in turn enables the feedback associated with the dissipation of the M_6 mode [i.e., $4bZ_1$ in Eq. (14)]. Although chaos may appear in the presence of nonlinearity as well as a heating term in the 3DLM, the increased degree of nonlinearity with additional dissipative terms (i.e., the extension of nonlinear feedback loop) in the 5DLM can reduce chaotic responses. Simply speaking, the appearance of small-scale processes that involve the nonlinear interactions with damping terms may help stabilize solutions. The role of the negative nonlinear feedback by $-XY_1$ was further demonstrated by parameterizing its effect into the revised 3DLMP. Based on the analysis of the analytical solutions for the critical points of the 5DLM, the negative nonlinear feedback process through $-XY_1$ is emulated by a nonlinear eddy dissipation term ($-qX^2$, $q \geq 0$). As the revised 3DLMP produces stable solutions as $25 \leq r \leq 40$, it is suggested that the predictability (or chaos) of the 3DLM can be improved (or suppressed) by the nonlinear dissipation term.

Since numerical solutions with the 5DLM display sensitive dependence on ICs after r is greater than 42.9, the butterfly effect of the first kind exists. As the 5DLM

(3DLM) contains only one horizontal and four (two) vertical wave modes, the predetermined nonlinear mode–mode interactions among the selected modes cannot generate any new modes and thus limit their spatial-scale interactions and upscale energy transfer. In addition, the inclusion of new modes could impact (i.e., increase) the stability of solutions in the 5DLM. Therefore, it is suggested that the appearance of the butterfly effect of the first kind cannot directly lead to the conclusion that small perturbations can alter large-scale structure, namely, the butterfly effect of the second kind, because 1) it requires further upscale transfer of energy by additional low-wavenumber modes and 2) the inclusion of new modes may have a significant impact on the solution stability (i.e., an extremely large r for the onset of chaos).

While chaotic solutions (associated with the butterfly effect of the first kind) occur in the low-dimensional LMs (e.g., 3DLM and 5DLM) that include very limited nonlinear-scale interactions (i.e., limited degree of nonlinearity), it was reported that stable solutions could be obtained in the "sufficiently high-resolution" model by Curry et al. (1984). Therefore, it is hypothesized that solution stability in high-dimensional LMs can be further increased through additional negative nonlinear feedback with additional modes in numerical modeling. However, the nonexistence of a nontrivial critical point in the 4DLM (as $r > d_o + 1$) may indicate the importance of proper mode truncation in improving the solution stability of the nonlinear system that has a finite degree of nonlinearity. Specifically, a comparison among the 3DLM, 4DLM, and 5DLM suggests that the inclusion of only the M_5 (e.g., Y_1) mode cannot effectively improve stability; while the inclusion of both the M_5 and M_6 modes can improve stability, the latter requires the former to help provide its feedback to the 3DLM through the new feedback loops, namely, $M_3 \rightarrow M_5 \rightarrow M_3$ and $M_5 \rightarrow M_6 \rightarrow M_5$. In addition, M_6 is required to conserve the domain-averaged total energy in the dissipationless limit. Therefore, we suggest that an incremental change in the degree of nonlinearity (e.g., with only M_5 mode) may not be a sufficient condition for improving stability particularly in the low-dimensional LMs. We will continue to examine this feature by incrementally increasing the number of modes in generalized LMs.

To achieve the above goals, we have derived a 6DLM with the inclusion of the M_4 mode [$M_4 = \sqrt{2}\sin(lx)\sin(3mz)$]. After finishing the derivations of the 6DLM in the fall of 2011, we became aware of the recent studies by Professor Z. E. Musielak and his colleagues who obtained the same 6DLM (Musielak et al. 2005). The 6DLM produces a slightly smaller r_c (=41.1) for chaotic solutions than the 5DLM. A comparison between the two LMs has been made to investigate the impact of an additional heating term associated with the M_4 mode on the solution's stability, which is in preparation for publication (Shen 2014, manuscript submitted to *J. Atmos. Sci.*). To improve our understanding of the chaos dynamics and thus the short-term predictability (e.g., Legras and Ghil 1985; Nese and Dutton 1993; Nese et al. 1996), we will address if and how the changes of the critical points in the revised 3DLMP and 5DLM, which have been solved analytically, can impact the transient evolution of chaotic solutions with respect to the original 3DLM. For example, the growth rate of the envelope of the numerical solutions (e.g., Fig. 4) from the nonlinear and linear systems in Eqs. (C2)–(C6) (with FN = 1 or 0) will be compared to the corresponding finite-time LE (e.g., Nese 1989; Zeng et al. 1991; Li and Ding 2011) and linear growth rate (e.g., Fig. 10). Fractal dimension in different LMs will be analyzed with different methods (e.g., Grassberger and Procaccia 1983; Nese et al. 1987; Zeng et al. 1992) to understand the solution's stability. Our ultimate goal is to apply these analysis methods to examine the dependence of the solution's stability on mesoscale resolutions (e.g., ¼° versus 1/12°) and on model physics (e.g., different moist processes) in global weather and climate simulations (Shen et al. 2006b, 2012).

Acknowledgments. We thank anonymous reviewers, Drs. Y.-L. Lin, R. Anthes, X. Zeng, R. Pielke, J. Dutton, A. Molod, H.-M. H. Juang, S. Cheung, C.-L. Shie, and Y.-L. Wu for their valuable comments and encouragement, Professor Z. Wu for providing the code for the calculation of Gaussian white noise, and Ms. J. Dunbar and K. Massaro for proofreading this manuscript. We are grateful for support from the NASA Advanced Information System Technology (AIST) program of the Earth Science Technology Office (ESTO) and from the NASA Computational Modeling Algorithms and Cyberinfrastructure (CMAC) program. Resources supporting this work were provided by the NASA High-End Computing (HEC) program through the NASA Advanced Supercomputing division at Ames Research Center. Special thanks are due to the library personnel of NASA GSFC Library for helping obtain a copy of several classical journal articles.

APPENDIX A

Energy Conservation in the 5DLM

The domain-averaged kinetic energy ($\overline{\mathrm{KE}}$) and potential energy ($\overline{\mathrm{PE}}$) are defined as follows (e.g., Treve and Manley 1982; Thiffeault and Horton 1996):

$$\overline{\mathrm{KE}} = \frac{1}{2}\int_0^{2H/a}\int_0^{H}(u^2 + w^2)\,dz\,dx, \qquad \text{(A1)}$$

$$\overline{\mathrm{PE}} = -\int_0^{2H/a}\int_0^H g\alpha(z\theta)\,dz\,dx. \tag{A2}$$

With Eqs. (7) and (9), Eq. (A1) becomes

$$\overline{\mathrm{KE}} = \frac{\pi^2}{2}\kappa^2\left(\frac{1+a^2}{a}\right)^3 X^2 = \frac{C_3}{2}X^2, \tag{A3}$$

where $C_3 = \pi^2\kappa^2[(1+a^2)/a]^3$. Since the integral of the M_2 and M_5 modes over the domain is equal to zero, $\overline{\mathrm{PE}}$ in Eq. (A2) is written as

$$\overline{\mathrm{PE}} = C_2 g\alpha\int_0^{2H/a}\int_0^H z(ZM_3 + Z_1M_6)\,dz\,dx,$$

and becomes

$$\overline{\mathrm{PE}} = -\pi^2\nu\kappa\left(\frac{1+a^2}{a}\right)^3\left(Z+\frac{Z_1}{2}\right) = -C_3\sigma\left(Z+\frac{Z_1}{2}\right). \tag{A4}$$

From Eqs. (A3) and (A4), the time derivative of the total energy is written as follows:

$$\frac{d\overline{\mathrm{KE}}}{d\tau} + \frac{d\overline{\mathrm{PE}}}{d\tau} = C_3\left[X\frac{dX}{d\tau} - \sigma\left(\frac{dZ}{d\tau} + \frac{dZ_1}{2d\tau}\right)\right]. \tag{A5}$$

To examine Eq. (A5) in the dissipationless limit ($\nu = \kappa = 0$), we derive the following equations by multiplying Eqs. (10), (12), and (14) of the 5DLM by X, $-\sigma$, and $-\sigma/2$, respectively,

$$X\frac{dX}{d\tau} = \cancel{-\sigma X^2} + \sigma XY, \tag{A6}$$

$$-\sigma\frac{dZ}{d\tau} = -\sigma XY + \sigma XY_1 + \cancel{\sigma bZ}, \tag{A7}$$

$$-\sigma\frac{dZ_1}{2d\tau} = -\sigma XY_1 + \cancel{2\sigma bZ_1}. \tag{A8}$$

Here the crossed-out symbol indicates a dissipative term that is associated with either $\nu\nabla^4\psi$ or $\kappa\nabla^2\theta$ in Eqs. (1) and (2). The dissipative terms are neglected in the dissipationless limit. The term σXY in Eq. (A6) is originally from the linear term $g\alpha(\partial\theta/\partial x)$ in Eq. (1), while the other nonlinear terms in Eqs. (A7) and (A8) are from the advection term $J(\psi,\theta)$ in Eq. (2). Equation (A6) represents the time derivative of the $\overline{\mathrm{KE}}$ and Eq. (A7) [Eq. (A8)] represents the time derivative of the $\overline{\mathrm{PE}}$. The nonlinear term XY, which appears in Eqs. (A6) and (A7), is responsible for the conversion of $\overline{\mathrm{KE}}$ and $\overline{\mathrm{PE}}$, while the nonlinear term XY_1 is responsible for the conversion of $\overline{\mathrm{PE}}$ at different scales. As the summation of Eqs. (A6)–(A8) is zero when the crossed-out terms are excluded, we have $d\overline{\mathrm{KE}}/dt + d\overline{\mathrm{PE}}/dt = 0$. Therefore, the total energy is conserved. Note that in the 3DLM where both Y_1 and Z_1 are missing in Eqs. (A7) and (A8), Eq. (A5) is still equal to zero. However, Z has to be included to conserve the total energy in the 3DLM. In comparison, when Z_1 is not in Eq. (A8) but only Y_1 is included in Eq. (A7), Eq. (A5) is not equal to zero, except for the trivial solution $X = 0$. Therefore, it is important to include both Y_1 and Z_1 (i.e., both M_5 and M_6 modes) to conserve the total energy of the system.

When dissipation terms are included in Eqs. (A6)–(A8), the time derivative of the total energy becomes

$$\frac{d\overline{\mathrm{KE}}}{d\tau} + \frac{d\overline{\mathrm{PE}}}{d\tau} = C_3\sigma(-X^2 + bZ + 2bZ_1). \tag{A9}$$

In the above equation, the nonlinear terms (XY and XY_1) are implicit while they are internally responsible for the energy conversion. When a steady state is reached, Eq. (A9) leads to $X_c[=\pm\sqrt{b(Z_c+2Z_{1c})}]$, which is the same as Eq. (19c). In addition, the M_1 mode is associated with $d\overline{\mathrm{KE}}/d\tau < 0$. When the mode M_3 has a positive (negative) amplitude, it is associated with negative (positive) potential energy [Eq. (A4)], but the corresponding tendency [$d\overline{\mathrm{PE}}/d\tau$ in Eq. (A9)] adds positive (negative) potential energy to the system. The M_6 plays a role similar to the M_3 mode.

APPENDIX B

Downscale and Upscale Transfer Processes in the Nonlinear Feedback Loop: A Simple Illustration

In this section, we use trigonometric functions to discuss the downscale and upscale transfer associated with the nonlinear Jacobian $J(\psi,\theta)$ term, both of which may form a nonlinear feedback loop. The Jacobian term can be written as $w\partial\theta/\partial z + u\partial\theta/\partial x$. The first and second terms represent the nonlinear vertical and horizontal advection of temperature, respectively. The four Jacobian terms in Eq. (28) are briefly analyzed below. With no loss of generality, we can assume two modes as $\sin(lx)\sin(pz)$ (e.g., M_1 or M_4) and $\cos(lx)\sin(qz)$ (e.g., M_2 or M_5) (or $\sin(qz)$, e.g., M_3 or M_6), respectively. Here p and q represent vertical wavenumbers: $p = m$ or $3m$ and $q = m$, $2m$, $3m$, or $4m$. Therefore, the corresponding Jacobian becomes

$$lq\cos^2(lx)\sin(pz)\cos(qz) + lp\sin^2(lx)\cos(pz)\sin(qz)$$

and is proportional to the following:

$$q\sin(pz)\cos(qz) + p\cos(pz)\sin(qz), \tag{B1}$$

when $\cos^2(lx) = [1 + \cos(2lx)]/2 \sim ½$ and $\sin^2(lx) = [1 - \cos(2lx)]/2 \sim ½$ because of the truncation of the horizontal wave modes. Equation (B1) is dominated by the first part (i.e., $w\partial\theta/\partial z$) when $p < q$ or by the second part (i.e., $u\partial\theta/\partial x$) when $p > q$. Since we are mainly concerned with the representation of $J(M_1, M_3)$ and subsequent nonlinear processes, we simply discuss the Jacobian of the M_1 and one of the other modes, which is represented dominantly by $\sin(pz)\cos(qz)$ because $p < q$. Thus we have

$$\sin(pz)\times\cos(qz) = \frac{1}{2}\{\sin[(p+q)z] - \sin[(q-p)z]\} \quad \text{as} \quad p<q. \tag{B2}$$

The above equation indicates that the nonlinear interaction could lead to the generation of two new wave modes with wavenumbers $(p + q)$ and $(q - p)$ or to the modification of these two modes if they already exist. Therefore, downscale and upscale transfer processes may occur. The appearance of the new mode at a higher wavenumber $(p + q)$ enables its subsequent interaction with the M_1 mode that leads to

$$\sin(pz)\times\cos[(p+q)z] = \frac{1}{2}[\sin(2p+q)z - \sin(q)z]. \tag{B3}$$

Therefore, Eqs. (B2) and (B3) collectively suggest that the "new" (or influenced) mode, $\sin[(p + q)z]$, generated (or modified) by the nonlinear downscale transfer process associated with the incipient wave mode $[\sin(qz)]$, can provide feedback to the incipient wave mode via a subsequent nonlinear upscale transfer process (as $q < p + q$). Thus, a feedback loop forms with Eqs. (B2) and (B3). Although these equations represent only the first part of the Jacobian function [e.g., Eq. (B1)], they are representative for $J(M_1, M_j)$, where $j = 2, 3, 5$, and 6, that includes all of the nonlinear terms for the 5DLM as well as the major nonlinear terms for the 6DLM (B.-W. Shen 2013, unpublished manuscript). More specific discussions are given sections 3a and 3b with the calculation of the Jacobian.

APPENDIX C

Numerical Method of the Stability Analysis near a Critical Point

The solutions with initial conditions near a nontrivial critical point are analyzed as follows. We decompose the total field into the basic part and perturbation, which can be written as

$$A = A_c + A', \tag{C1}$$

where A represents (X, Y, Z, Y_1, or Z_1), A_c represents the basic state that is from the solution of the critical point, and A' is a perturbation that measures the departure from the critical point. With Eq. (C1), the 5DLM [Eqs. (10)–(14)] becomes

$$\frac{dX'}{d\tau} = -\sigma X' + \sigma Y', \tag{C2}$$

$$\frac{dY'}{d\tau} = (r - Z_c)X' - Y' - X_cZ' - \mathrm{FN}(X'Z'), \tag{C3}$$

$$\frac{dZ'}{d\tau} = (Y_c - Y_{1c})X' + X_cY' - bZ' - X_cY_1' + \mathrm{FN}(X'Y' - X'Y_1'), \tag{C4}$$

$$\frac{dY_1'}{d\tau} = (Z_c - 2Z_{1c})X' + X_cZ' - dY_1' - 2X_cZ_1' + \mathrm{FN}(X'Z' - 2X'Z_1'), \tag{C5}$$

$$\frac{dZ_1'}{d\tau} = 2Y_{1c}X' + 2X_cY_1' - 4bZ_1' + 2\mathrm{FN}(X'Y_1'). \tag{C6}$$

Here the flag FN indicates if the system is fully nonlinear (FN = 1) or not (FN = 0). The system with FN = 0 is linear with respect to the critical point. However, as the solutions of the basic state (critical point) are from the time-independent nonlinear 5DLM, the "linear system" with FN = 0 still poses the nonlinearity of the basic state. Numerical solutions with FN = 1 and FN = 0 will be compared to understand the evolution of solution's growth rates that are impacted by the nonlinearity. Here, for local stability analysis, we only consider Eqs. (C2)–(C6) with FN = 0, which can be written as follows:

$$\frac{d\mathbf{s}}{d\tau} = \mathbf{A}\mathbf{s}, \tag{C7}$$

where $\mathbf{s}$ and $\mathbf{A}$ are a column vector and matrix, respectively. The term $\mathbf{s}$ is (X, Y, Z, Y_1, and Z_1), and the matrix $\mathbf{A}$ for the 5DLM, denoted $\mathbf{A}^{5d}$ is written as follows:

$$\mathbf{A}^{5d} = \begin{pmatrix} -\sigma & \sigma & 0 & 0 & 0 \\ r - Z_c & -1 & -X_c & 0 & 0 \\ Y_c - Y_{1c} & X_c & -b & -X_c & 0 \\ Z_c - 2Z_{1c} & 0 & X_c & -d & -2X_c \\ 2Y_{1c} & 0 & 0 & 2X_c & -4b \end{pmatrix}.$$

Similarly, the matrix $\mathbf{A}$ with the nontrivial critical point for the 3DLM and 3DLMP are denoted $\mathbf{A}^{3d}$ and $\mathbf{A}^{r3d}$, defined as follows:

$$\mathbf{A}^{3d} = \begin{pmatrix} -\sigma & \sigma & 0 \\ r - Z_c^{3d} & -1 & -X_c^{3d} \\ Y_c^{3d} & X_c^{3d} & -b \end{pmatrix},$$

$$\mathbf{A}^{r3d} = \begin{pmatrix} -\sigma & \sigma & 0 \\ r - Z_c^{r3d} & -1 & -X_c^{r3d} \\ Y_c^{r3d} - 2qX_c^{r3d} & X_c^{r3d} & -b \end{pmatrix}.$$

The critical points are analytically defined in Eq. (21) for the 3DLM, in Eq. (22) for the 3DLMP, and in Eq. (19) for the 5DLM. By assuming $\mathbf{s} = s_o e^{\lambda\tau}$, we obtain the following characteristic equation:

$$\mathbf{A}\mathbf{s} = \lambda \mathbf{I}\mathbf{s}, \tag{C8}$$

where λ is the eigenvalue of the system and $\mathbf{I}$ is the identity matrix. The number of eigenvalues is equal to the number of the dimensions in these LMs, and each of these eigenvalues can be a real or complex number. Let $\mathrm{Re}(\lambda)$ represent the real part of λ, so the appearance of a positive $\mathrm{Re}(\lambda)$ suggests an unstable solution near the critical point. Given any pair of (σ, r), we calculate the eigenvalues by solving Eq. (C8) using EISPACK (e.g., Smith et al. 1976) (http://www.netlib.org/eispack/) and only analyze the maximum value of $\mathrm{Re}(\lambda)$. Figure 10 shows the results of the $\mathrm{Re}(\lambda)$ in the (σ, r) space where $5 \le \sigma \le 25$ with $\Delta\sigma = 0.01$ and $20 \le r \le 50$ with $\Delta r = 0.01$. Discussions are made in section 3e.

REFERENCES

Anthes, R., cited 2011: Turning the tables on chaos: Is the atmosphere more predictable than we assume? NCAR/UCAR AtmosNews. [Available online at https://www2.ucar.edu/atmosnews/opinion/turning-tables-chaos-atmosphere-more-predictable-we-assume-0.]

Atlas, R., and Coauthors, 2005: Hurricane forecasting with the high-resolution NASA finite volume general circulation model. *Geophys. Res. Lett.,* **32,** L03801, doi:10.1029/2004GL021513.

Bender, C. M., and S. A. Orszag, 1978: *Advanced Mathematical Methods for Scientists and Engineers.* McGraw-Hill, 593 pp.

Biswas, R., M. J. Aftosmis, C. Kiris, and B.-W. Shen, 2007: Petascale computing: Impact on future NASA missions. *Petascale Computing: Architectures and Algorithms,* D. Bader, ed., Chapman and Hall/CRC Press, 29–46.

Christiansen, F., and H. Rugh, 1997: Computing Lyapunov spectra with continuous Gram-Schmid orthonormalization. *Nonlinearity,* **10,** 1063–1072.

Curry, J. H., 1978: Generalized Lorenz systems. *Commun. Math. Phys.,* **60,** 193–204.

——, J. R. Herring, J. Loncaric, and S. A. Orszag, 1984: Order and disorder in two- and three-dimensional Benard convection. *J. Fluid Mech.,* **147,** 1–38.

Ding, R. O., and J. P. Li, 2007: Nonlinear finite-time Lyapunov exponent and predictability. *Phys. Lett.,* **354A,** 396–400.

Eckhardt, B., and D. Yao, 1993: Local Lyapunov exponents in chaotic systems. *Physica D,* **65,** 100–108.

Froyland, J., and K. H. Alfsen, 1984: Lyapunov-exponent spectra for the Lorenz model. *Phys. Rev.,* **29A,** 2928–2931.

Gleick, J., 1987: *Chaos: Making a New Science.* Penguin, 360 pp.

Grassberger, P., and I. Procaccia, 1983: Characterization of strange attractors. *Phys. Rev. Lett.,* **5,** 346–349.

Kaplan, J. L., and J. A. Yorke, 1979: Chaotic behavior of multidimensional difference equations. *Functional Differential Equations and the Approximations of Fixed Points,* H. O. Peitgen and H. O. Walther, Eds., Lecture Notes in Math, Vol. 730, Springer-Verlag, 204–227.

Kazantsev, E., 1999: Local Lyapunov exponents of the quasi-geostrophic ocean dynamics. *Appl. Math. Comput.,* **104,** 217–257.

Legras, B., and M. Ghil, 1985: Persistent anomalies, blocking, and variations in atmospheric predictability. *J. Atmos. Sci.,* **42,** 433–471.

Li, J., and R. Ding, 2011: Temporal-spatial distribution of atmospheric predictability limit by local dynamical analogs. *Mon. Wea. Rev.,* **139,** 3265–3283.

Lorenz, E., 1963a: Deterministic nonperiodic flow. *J. Atmos. Sci.,* **20,** 130–141.

——, 1963b: The predictability of hydrodynamic flow. *Trans. N. Y. Acad. Sci.,* **25,** 409–432.

——, 1972: Predictability: Does the flap of a butterfly's wings in Brazil set off a tornado in Texas? *Proc. 139th Meeting of AAAS Section on Environmental Sciences, New Approaches to Global Weather: GARP,* Cambridge, MA, AAAS, 5 pp. [Available online at http://eaps4.mit.edu/research/Lorenz/Butterfly_1972.pdf.]

Musielak, Z. E., D. E. Musielak, and K. S. Kennamer, 2005: The onset of chaos in nonlinear dynamical systems determined with a new fractal technique. *Fractals,* **13,** 19–31.

Nese, J. M., 1989: Quantifying local predictability in phase space. *Physica D,* **35,** 237–250.

——, and J. A. Dutton, 1993: Quantifying predictability variations in a low-order ocean atmosphere model: A dynamical systems approach. *J. Climate,* **6,** 185–204.

——, ——, and R. Wells, 1987: Calculated attractor dimensions for low-order spectral models. *J. Atmos. Sci.,* **44,** 1950–1972.

——, A. Miller, and J. A. Dutton, 1996: The nature of predictability enhancement in a low-order ocean-atmosphere model. *J. Climate,* **9,** 2167–2172.

Pielke, R., cited 2008: The real butterfly effect. [Available online at http://pielkeclimatesci.wordpress.com/2008/04/29/the-real-butterfly-effect/.]

Press, W. H., S. A. Teukolsky, W. T. Vetterling, and B. P. Flannery, 1992: *Numerical Recipes in C.* Cambridge University Press, 994 pp.

Roy, D., and Z. E. Musielak, 2007a: Generalized Lorenz models and their routes to chaos. I. Energy-conserving vertical mode truncations. *Chaos Solitons Fractals,* **32,** 1038–1052.

——, and ——, 2007b: Generalized Lorenz models and their routes to chaos. II. Energy-conserving horizontal mode truncations. *Chaos Solitons Fractals,* **31,** 747–756.

——, and ——, 2007c: Generalized Lorenz models and their routes to chaos. III. Energy-conserving horizontal and vertical mode truncations. *Chaos Solitons Fractals,* **33,** 1064–1070.

Saltzman, B., 1962: Finite amplitude free convection as an initial value problem. *J. Atmos. Sci.,* **19,** 329–341.

Shen, B.-W., R. Atlas, J.-D. Chern, O. Reale, S.-J. Lin, T. Lee, and J. Chang, 2006a: The 0.125 degree finite-volume general mesoscale circulation model: Preliminary simulations of mesoscale vortices. *Geophys. Res. Lett.,* **33,** L05801, doi:10.1029/2005GL024594.

——, ——, O. Reale, S.-J. Lin, J.-D. Chern, J. Chang, C. Henze, and J.-L. Li, 2006b: Hurricane forecasts with a global mesoscale-resolving model: Preliminary results with Hurricane Katrina (2005). *Geophys. Res. Lett.,* **33,** L13813, doi:10.1029/2006GL026143.

——, W.-K. Tao, and B. Green, 2011: Coupling advanced modeling and visualization to improve high-impact tropical weather prediction. *IEEE Comput. Sci. Eng.,* **13** (5), 56–67, doi:10.1109/MCSE.2010.141.

——, ——, Y.-L. Lin, and A. Laing, 2012: Genesis of twin tropical cyclones as revealed by a global mesoscale model: The role of mixed Rossby gravity waves. *J. Geophys. Res.,* **117,** D13114, doi:10.1029/2012JD017450.

Smith, B., J. Boyle, J. Dongarra, B. Garbow, Y. Ikebe, V. Klema, and C. Moler, 1976: *Matrix Eigensystem Routines—EISPACK Guide.* Lecture Notes in Computer Science, Vol. 6, Springer Verlag, 551 pp.

Solomon, S., D. Qin, M. Manning, Z. Chen, M. Marquis, K. Averyt, M. Tignor, and H. L. Miller Jr., Eds., 2007: *Climate Change 2007: The Physical Science Basis.* Cambridge University Press, 996 pp.

Sprott, J. C., 2003: *Chaos and Time-Series Analysis.* Oxford University Press, 528 pp.

Thiffeault, J.-L., and W. Horton, 1996: Energy-conserving truncations for convection with shear flow. *Phys. Fluids,* **8,** 1715–1719.

Treve, Y. M., and O. P. Manley, 1982: Energy conserving Galerkin approximations for 2-D hydrodynamic and MHD Benard convection. *Physica D,* **4,** 319–342.

Wolf, A., J. B. Swift, H. L. Swinney, and J. A. Vastano, 1985: Determining Lyapunov exponents from a time series. *Physica D,* **16,** 285–317.

Zeng, X., R. Eykholt, and R. A. Pielke, 1991: Estimating the Lyapunov-exponent spectrum from short time series of low precision. *Phys. Rev. Lett.,* **66,** 3229–3232.

——, R. A. Pielke, and R. Eykholt, 1992: Estimate of the fractal dimension and predictability of the atmosphere. *J. Atmos. Sci.,* **49,** 649–659.